Preprints.org

Article

Not peer-reviewed version

Preprocessing of Retinal Fundus Image Using Clifford Algebra

Somasis Roy *, Anirban Mitra, Sanjit Kumar Setua

Posted Date: 11 May 2026

doi: 10.20944/preprints202605.0666.v1

Keywords: Clifford Algebra; retinal fundus images; multivector; bivector; RGB color model; gray level axis; enhancement

Preprints.org is a free multidisciplinary platform providing preprint service that is dedicated to making early versions of research outputs permanently available and citable. Preprints posted at Preprints.org appear in Web of Science, Crossref, Google Scholar, Scilit, Europe PMC, OpenAlex.

Copyright: This open access article is published under a Creative Commons CC BY 4.0 license, which permit the free download, distribution, and reuse, provided that the author and preprint are cited in any reuse.

Preprints.org (www.preprints.org) | NOT PEER-REVIEWED | Posted: 11 May 2026 doi:10.20944/preprints202605.0666.v1

Disclaimer/Publisher's Note: The statements, opinions, and data contained in all publications are solely those of the individual author(s) and contributor(s) and not of MDPI and/or the editor(s). MDPI and/or the editor(s) disclaim responsibility for any injury to people or property resulting from any ideas, methods, instructions, or products referred to in the content.

Article

Preprocessing of Retinal Fundus Image Using Clifford Algebra

Somasis Roy [1,*], Anirban Mitra [2] and Sanjit Kumar Setua [1]

[1] Dept. of Computer Science & Engineering, Calcutta University Technology Campus, JD-2, Sector-III, Salt Lake, Kolkata 700098, India

[2] Dept. of Computer Science & Engineering, Sister Nivedita University, DG 1/2 Newtown Action Area 1, Kolkata – 700156, West Bengal, India

* Correspondence: somasis.roy@gmail.com

Abstract

This research presents a novel approach for enhancing retinal fundus images to detect anomalies better and diagnose retinal diseases. The work is divided into two stages: image representation and enhancement. Fundus images are represented in a Clifford color space, a 3D color model based on the RGB system, where colors are stored as multivectors that preserve color information and luminance. A rotation operation is applied to correct the image's illumination by adjusting brightness and color deviations, with the rotation angle and axis being critical for accurate enhancement. The gray-level axis serves as the rotational plane and the rotational angle of $\frac{4\pi}{3}$with a grayscale bivector axis, determined via discrete entropy (DE), optimally corrects image illumination. Following this, the green channel is extracted and enhanced using the CLAHE technique before being recombined with the other channels, and the image is reverse-rotated to its original color space. The effectiveness of the proposed method is evaluated using PSNR, DE, and SSIM on the MESSIDOR and DRIVE datasets, showing superior image quality and information preservation compared to existing methods. This enhanced technique is particularly beneficial for retinal landmark and lesion detection, improving diagnostic accuracy in retinal imaging.

Keywords: Clifford Algebra; retinal fundus images; multivector; bivector; RGB color model; gray level axis; enhancement

1. Introduction

The human eye collects most information to lead a healthy everyday life. The human brain is most often engaged in analyzing information received and its correct application. This information is mainly directed to the human body for physical and mental performance. Any eye problem is critical in that case, reducing various bodily functions. Eye-related diseases can be resolved promptly with appropriate monitoring and medical procedures. The first step in determining these diseases is observing the interstitial formation of the eye. This observation is directly dependent on the computer-generated retinal image. The features of various eye-related diseases are captured using standard imaging techniques like the Fundus camera and OCT.

Many critical disorders appear in the retina; retinal fundus imaging has been widely used in traditional diagnostics. Ophthalmologists commonly use retinal fundus images to diagnose certain retinal disorders. The images reveal pathological changes that could indicate disorders of the eye or cardiovascular system, such as diabetic retinopathy, age-related macular degeneration, arteriosclerosis, and so on. A color retinal fundus image at the early stage of disease may prevent the visual disorder of a patient by its powerful imaging expression. The image expresses the existing state of some essential features of the retina, like the optic disc, optic cup, fovea, exudates, and blood vessels. These features are likely to be tormented by abnormalities. Poor handling of complicated imaging environments, pupil dilation, and unanticipated eye movements are observed in many

© 2026 by the author(s). Distributed under a Creative Commons CC BY license.

Preprints.org (www.preprints.org) | NOT PEER-REVIEWED | Posted: 11 May 2026 doi:10.20944/preprints202605.0666.v1

retinal images of clinically disappointing quality. Two of the most significant issues obstructing clinical diagnosis using fundus images are uneven illumination and low contrast. Excellent quality of fundus images is crucial for further image processing steps such as vascular segmentation, optic disc localization, and color lesion detection.

Quality retinal fundus images are widely used manually or without human intervention to identify and analyze various diseases depicted in Figure 1(a). Several issues can arise with retinal fundus images, reducing their quality and interpretability. These difficulties include poor contrast, low resolution, noise from numerous sources such as sensor artifacts or speckle noise, uneven illumination, distortions caused by eye movements or lens flaws, and the presence of occlusions such as eyelashes or dust particles shown in Figure 1(b) – (f). Variations in imaging settings and equipment can also cause color balance and intensity variances among images, making accurate analysis and diagnosis complex. These difficulties highlight the significance of preprocessing approaches in addressing these concerns and improving the usability of retinal fundus pictures for clinical assessment and research reasons.

Figure 1. Retinal image instances. (a) High-quality image. (b) Blur. (c) Low illumination. (d) High illumination. (e) Uneven illumination. (f) Color distortion.

Preprocessing is indispensable in retinal fundus image analysis as it is a foundational step to enhance image quality and ensure accurate interpretation. Preprocessing techniques modify the raw images by addressing noise reduction, contrast enhancement, normalization, artifact removal, image registration, and segmentation, allowing subtle details such as blood vessels, optic discs, and lesions to become more visible and detectable. This refinement helps clinicians make a better diagnosis and helps automated analytic systems find and quantify problems. Furthermore, preprocessing standardizes image appearance across datasets, allowing for uniform analysis and comparison, longitudinal studies, and multimodal image fusion to provide a more complete assessment of retinal pathology. Thus, preprocessing is an essential preliminary step in improving retinal fundus images for future clinical evaluation.

The quality of retinal fundus images significantly impacts the accuracy of subsequent analysis. Managing variables like lighting, focus, and resolution when taking images is essential to guarantee clear and detailed images. Therefore, RFI representation with a suitable color model is crucial before proceeding to the enhancement steps. Many literatures adopted existing color models such as RGB [1], HSI [2], and Lab [3] to establish their procedural approaches for accurate image analysis.

Several types of enhancement techniques are applied for retinal fundus image analysis. The procedures can be classified into several categories: transform-based functions, color space conversion and normalization, filter-based, statistical histogram-based, learning-based, and vector-based image enhancement, which will be discussed in the literature review section. In contrast, these techniques have shown effectiveness for specific tasks such as retinal landmark detection and lesion segmentation for disease screening. However, they lack a unified representation and enhancement tool capable of streamlining subsequent computational steps into a single pass for more efficient processing.

Clifford Algebra (CA), also known as Geometric Algebra, emerged as a robust mathematical framework in computer vision, computer graphics, medical image processing, etc. [4]. It is popular as a unified geometric framework due to its recognized brilliance of operator's application,

© 2026 by the author(s). Distributed under a Creative Commons CC BY license.

Preprints.org (www.preprints.org) | NOT PEER-REVIEWED | Posted: 11 May 2026 doi:10.20944/preprints202605.0666.v1

comprehensive representation, and the solution to geometric hassle [5]. It can represent an RGB image using a powerful tool called a multivector. The RGB color channel against each pixel is defined as a single entity or multivector. This algebra is enriched with a set of geometric operators that have the skill to perform various image-processing procedures with lesser computational overheads [6]. With the aid of CA, the fundus image is represented as a color multivector image in place of an RGB image.

Every color pixel in RFI is expressed as an intersection of three primary color planes in $\mathbf{3}\mathbb{D}$ RGB color space. CA plots the whole color space into $\mathbf{3}\mathbb{D}$ Clifford space ($\boldsymbol{\mathcal{C}l_3}$) instead of Euclidean vector space [5]. Each of the color planes is the $\mathbf{2}\mathbb{D}$ oriented subspace known as the bivector. Hence, the colors are described in terms of bivector in $\boldsymbol{\mathcal{C}l_3}$ space. The two characteristics are the colors' chromaticity or hue and the intensity or brightness. Notably, the chromaticity and intensity of a color are defined respectively by the direction and magnitude of a color vector. CA is well equipped by its operators to express both color features. The rotor operator is beneficial for rotating a multivector in any dimension of the Clifford space. The color bivector ($\mathbf{Grade} - \mathbf{2}$ multivector) is rotated using a rotor operator in the space to generate a new nature of the color. The angle of rotation and rotation axis spanned by the bivector basis determines the color features. The change in the intensity feature of a color due to rotation affects the brightness. Similarly, the purity of a color is changed by rotation, which influences the color representation of an image. Reverse rotor operation is the rotation of the color bivector to the reverse angle to preserve chromatic or color features.

In RFI, the color is the best descriptor of different lesions such as Microaneurysm (small red dot), Hard exudate (solid yellow pigment), Haemorrhage (dark red patch), soft exudate (light yellow dot) according to the ophthalmologists. An exact segmentation of these lesions is reliant on the contrast adjustment. The color brightness difference between the retinal background and anatomical structure is required to be more consistent. Every pixel in RFI is consistently improved to enable accurate medical detection of various eye-related diseases.

With the aid of CA, the fundus image is represented as a color multivector image in place of an RGB image. The change in $\mathbf{Grade} - \mathbf{2}$ color multivector for a certain angle of rotation in $\boldsymbol{\mathcal{C}l_3}$space has a resemblance with the Hue-Saturation feature in HSI space. The rotation angle along the rotational axis determines color intensity, similar to a pixel's brightness value. The primary colors in HSI space are situated $\mathbf{120°}$ apart from each other. Any rotation lesser than $\mathbf{45°}$ will reduce the brightness of the color is theoretically proved and experimented. The relationship between the angle of rotation and color brightness is established by CA, and an increase in rotating angle larger than $\mathbf{45°}$ causes a growth in brightness. The rotating axis is another factor determining the intensity to be increased. The bivector basis has been selected among numerous grades of multivector as the rotational axis in color multivector rotor operation [7]. This basis behaves similarly to the grey level axis in HSI space. A measurement of the improved color brightness multivector is made after rotation. The contrast adjustment is managed using the CLAHE algorithm, which receives the quantized luminous value of each pixel represented as vectors ($\mathbf{Grade} - \mathbf{2}$ multivector). The reverse rotation in Clifford space preserves the chromaticity feature of the color with enhanced intensity and contrast behavior. The fundus image is enhanced to avoid the loss of retinal features and preserve the original colorfulness. It displays CA's capacity to represent RFI utilizing a color multivector while enhancing and guaranteeing that the challenges posed by anatomical colorfulness and varied color model conversion are successfully disabled.

This literature introduces an alternative representation of RFI using the CA multivector operator. It illustrates the variety of rotational impacts on the retinal image using a rotor operator. The proposed image enhancement technique is designed to maintain the fundamental characteristics of the retinal anatomy. It ensures that no crucial information is lost or distorted during preprocessing. Moreover, the method avoids introducing artificial elements or noise, which can compromise the accuracy of subsequent image analysis. Significantly, this approach operates independently of prior knowledge about specific retinal structures, making it adaptable to various image conditions. By establishing a solid foundation through effective preprocessing, the subsequent stages of image

© 2026 by the author(s). Distributed under a Creative Commons CC BY license.

Preprints.org (www.preprints.org) | NOT PEER-REVIEWED | Posted: 11 May 2026 doi:10.20944/preprints202605.0666.v1

analysis, such as anatomical structure segmentation and feature extraction, can be performed with better reliability.

A novel method is proposed in this literature for enhancement of the retinal fundus image using Clifford Algebra. It describes the enhancement in two steps, in which color multivectors are rotated for luminosity improvement first. In the second step, the contrast of the color multivectors is corrected using conventional CLAHE. The proposal works on the MESSIDOR and DRIVE datasets available online. The rest of the paper is organized as follows. Section 2 discusses the various types of research on RFI enhancement using multiple color models in conventional frameworks and learning-based approaches in recent years. Retinal fundus image representation using Clifford Algebra & its operators are introduced in section 3. Section 4 discusses the mathematics behind the Clifford color space for the foundation of the fundus image. Section 5 explains the newly introduced Clifford color space-based retinal fundus image representation. Section 6 explores the enhancement method by the rotor operator of CA applied on a retinal image. The experimental results for two datasets and performance evaluations compared to existing methods are extensively discussed in sections 7 and 8, respectively. Conclusion and future scope discoveries round-up in section 9 finish this work.

2. Related Work

The quality of retinal fundus images profoundly influences the precision of subsequent analyses. These images must be clear and detailed to provide accurate information for further examination. Achieving such clarity and detail depends on effectively controlling various factors during the image capture, such as lighting conditions, focus sharpness, and image resolution. Representing retinal fundus images using an appropriate color model for detail analysis is crucial. This step is essential before any preprocessing, as the color model affects how image data is interpreted and processed. Many researchers have recognized the importance of this initial step and adopted existing color models in their studies. Doing so establishes a robust foundation for their analytical procedures, ensuring the images are accurately represented and ready for further examination. These color models help to maintain consistency and accuracy across different stages of image analysis, ultimately leading to more reliable results.

The author of [1] emphasized that a suitable color model must represent retinal fundus images before preprocessing can be performed. It should be mentioned that several academics have used pre-existing color models in their work to create reliable procedures for precise image analysis. The significance of utilizing the RGB color model among various color models in image enhancements to preserve consistency and reliability in image analysis is covered in the literature [8]. Their approach offers a foundation for improving retinal images, which can be useful for precise research and diagnosis. This enhancement framework [9] for Diabetic Retinopathy detection is designed to ensure that the images are clear and detailed, essential for accurate analysis and diagnosis. The authors suggest that choosing an RGB color model that appropriately depicts retinal images is necessary before initiating any preprocessing procedures. By guaranteeing the reliability and uniformity of image processing, this technique helps produce more accurate diagnoses. Alwazzan et al. [10] proposed a hybrid approach to enhance the quality of color retinal fundus images. The method considers the RGB color model and separates each color channel. Green channels are targeted for enhancement, which suffers from noise and low contrast. This approach applied CLAHE on the green color channel for contrast improvement. This literature focused on improved visualization of blood vessels and other significant features for retinal disease diagnosis. This literature [11] proposed the importance of image quality in precise color lesion detection. It focused on selecting the HSI color model among several models for proper retinal image enhancement to improve the clarity and detailing of the diseased and non-diseased images. In [12], the authors focused on appropriate image representation and preprocessing for detecting vascular intersection in retinal fundus images. The HSI model ensures the proper management of factors while achieving reliable vascular intersection and analysis. HSV-based characteristics have been studied for applications such as optic disc and cup segmentation, where color and intensity differences are essential for differentiating between

© 2026 by the author(s). Distributed under a Creative Commons CC BY license.

Preprints.org (www.preprints.org) | NOT PEER-REVIEWED | Posted: 11 May 2026 doi:10.20944/preprints202605.0666.v1

anatomical parts [8]. Due to its perceptual homogeneity, HSV is favored for tasks that call for color-based segmentation and analysis in retinal fundus images. This literature [13] introduced a novel image enhancement technique to improve the luminosity and contrast of the color retinal image. The algorithm is proposed in two stages comprising luminosity enhancement and contrast. The gamma correction method is applied to the value channel of the HSV color model, generating a luminosity gain matrix that enhances the illumination of the entire image. It results in improved visibility of retinal vessel details. In [14], the authors introduced a hybrid enhancement method that enhanced the whole image brightness on HSV color space but contrast correction locally. The final enhanced image is formed in the Lab* color space using CLAHE. Visual and quantitative evaluations establish the method's usefulness, improving image quality while preserving essential details. In [15], the proposed algorithm segments the retinal region from the rest of the image. The identified region undergoes enhancement within the Lab color space. The brightness component (L) is enhanced using adaptive histogram equalization while preserving the color information represented by the a and b channels. This research [16] focused on creating realistic retinal fundus images for analysis and testing. The method involves enhancing image contrast and color balance. The CLAHE technique is applied within the CIE Lab* color space, designed explicitly for perceptual color calculations to improve the contrast locally in the image. The authors aim to generate pictures that closely resemble real-world retinal images, facilitating the development and evaluation of image analysis algorithms.

The basic information of the fundus image background is obtained with the help of normalized convolution with domain transform function [17]. The enhanced image is retrieved after fusing the original image and acquired information. Curvelet transformation and adaptive sigmoid mapping of histogram equalization are used in a proposed hybrid approach to enhance and denoise retinal fundus images [18]. Modified sigmoid transformation is introduced to improve retinal fundus images' brightness in peripheral regions [19]. Many works of literature have found color space conversion as an inevitable step for preprocessing retinal fundus images. Instead of processing the pixels' perceived relative color values, the transformed color spaces merely process the pixels' intensity [20]. Similarly, in another literature [8,21], both the color spaces are deployed as preprocessing steps for the segmentation of retinal features. The 2D Gabor kernel function improves retinal vessels [22]. This Filter increases the contrast between vessel pixels and foundation pixels [23]. Morphological filters are also well-known techniques used for vessel enhancement [24]. In [25], Edge-based Texture Histogram Equalization (ETHE) was introduced to correct uneven illumination and poor contrast of the retinal fundus image. Pixel color amplification [26] improved retinal fundus images using amplification theory and enhancement methods to aid in fundus image segmentation. Gupta et al. [3] presented an algorithm for enhancing retinal fundus images in which contrast enhancement is carried out by quantile-based histogram equalization and the Adaptive Gamma Correction (AGC) process for brightness improvement.

Over the past few years, learning-based methods have gained significant popularity in medical image processing. These methods have been widely applied in tasks like image classification, image segmentation, object detection, and localization [27]. The authors proposed a method that combines support vector machine and mathematical morphology to achieve satisfactory classification accuracy in the filtered retinal image dataset [28]. The literature [29] employed a combination of vascular extraction and arteriovenous identification, utilizing the U-Net semantic segmentation structure to achieve arteriovenous segmentation in fundus images. Meanwhile, [30] used the support vector machine to detect the optic disc, facilitating further diagnosis of Glaucoma. These studies in retinal image processing are most effective when dealing with clear, high-contrast images that can be processed automatically, particularly on high-quality retinal image datasets. In contrast, [31] introduced a data-driven approach to enhance blurry retinal images. However, general datasets often contain various other causes of low-quality images beyond just blur, which hampers the feasibility of processing retinal images. In a previous study [32], low-quality images with artificial noise were improved without differentiating between different quality categories. Convolutional neural

© 2026 by the author(s). Distributed under a Creative Commons CC BY license.

Preprints.org (www.preprints.org) | NOT PEER-REVIEWED | Posted: 11 May 2026 doi:10.20944/preprints202605.0666.v1

networks can quickly learn this synthetic noise, but it fundamentally differs from the low-quality images captured by the fundus camera.

A new approach to retinal vascular segmentation is established in [33], which uses vector-based methods to improve vessel properties and accomplish accurate segmentation through local vessel structures. Researchers present a method in [34] for improving retinal vasculature by combining vector-based filters with local binary patterns. This helps with segmentation and analysis tasks by successfully emphasizing vascular architecture. In [35], a novel technique for optic disc detection in retinal pictures is reviewed. It uses vector-based procedures to enhance optic disc visibility and guarantee precise detection. A retinal vascular segmentation approach based on L1 regularized deep sparse filtering is presented in [36], which integrates vector-based filtering to improve vessel structures and provide robust segmentation results by efficiently suppressing background elements and noise. The combination of optic disc identification with vector-based enhancement approaches and machine learning algorithms accurately locate the optic disc in retinal images is investigated in [37]. The studies above highlight the significance of utilizing image representation and enhancement techniques in different areas of retinal image analysis, such as optic disc detection, vessel segmentation, and feature enhancement.

3. Clifford Algebra and Its Operators

Clifford Algebra was invented by William K. Clifford in 1876 as a method of quaternion generalization to higher dimensions. CA offers an invertible, associative product called a Geometric Product ($\mathbf{GP}$), which combines a dot product and an outer product. This algebra is a robust framework with integrated features like complex numbers, projective geometry, coordinate geometry, and linear algebra. Quaternion algebra is another wing of CA that incorporates the concept of subspaces. The conventional concept of linear algebra is extended towards CA, considering a set of subspaces and operators [7]. CA is a coordinate-free tool, and it is easier to model geometric objects and their transformations. Compared to linear algebra, it treats vectors as $\mathbf{1}\mathbb{D}$ subspaces and scalars as $\mathbf{0}\mathbb{D}$ (zero) subspaces. CA replaces the dot and cross products with inner & outer (or wedge) products. The subspaces of any dimension are called *blades*. A blade representing a certain $k-$dimensional subspace with k number of basis vectors describing it is called $\mathbf{Grade}-\mathbf{k}$ ($\mathcal{G}_{\mathbf{k}}$) vectors. A blade of $\mathbf{2}\mathbb{D}$ subspaces is $\mathbf{Grade}-\mathbf{2}$ ($\mathcal{G}_{\mathbf{2}}$) vectors or *bivector*. Similarly, a blade of $\mathbf{3}\mathbb{D}$ subspaces is a $\mathbf{Grade}-\mathbf{3}$ ($\mathcal{G}_{\mathbf{3}}$) vectors or *trivectors*. The blades are defined as a new type of product known as outer product or wedge product. A bivector represents the oriented area spanned by two vectors as a wedge product. Similarly, a trivector represents volume spanned by three vectors.

A. Fundamental Theory

A Euclidean vector space $\mathbb{V}^{\mathbf{n}}$ of $\mathbf{n}$ dimension is considered where its orthonormal basis vectors are $\mathbf{e_0}, \mathbf{e_1}, \mathbf{e_2}, \ldots . \mathbf{e_{n-1}}$. The subspaces are derived from the vector space $\mathbb{V}^{\mathbf{n}}$ by using CA. A corresponding $\mathbf{n}$-dimensional Clifford space $\mathcal{C}\mathbf{l_n}$ is formed where subspaces are basis elements. It is composed of $\mathbf{2^n}$ blades or subspaces. For example, $\mathcal{C}\mathbf{l_2}$ space has four basis blades $\{\mathbf{1}, \mathbf{e_1}, \mathbf{e_2}, \mathbf{e_1} \wedge \mathbf{e_2}\}$ and similarly $\mathcal{C}\mathbf{l_3}$ space is composed of eight basis blades $\{\mathbf{1}, \mathbf{e_1}, \mathbf{e_2}, \mathbf{e_3}, \mathbf{e_1} \wedge \mathbf{e_2}, \mathbf{e_2} \wedge \mathbf{e_3}, \mathbf{e_1} \wedge \mathbf{e_3}, \mathbf{e_1} \wedge \mathbf{e_2} \wedge \mathbf{e_3}\}$. The highest dimension basis blades are bivector and trivector in $\mathbf{2}\mathbb{D}$ and $\mathbf{3}\mathbb{D}$, respectively. These basis blades are known as *pseudoscalar* and are denoted with $\mathbf{I}$ in CA.

The geometric product of a basis blade to itself results in **+1**, **-1**, **0**. It suggests that there are nonnegative integers $\mathbf{p}$, $\mathbf{q}$ & $\mathbf{r}$ such that $\mathbf{n} = \mathbf{p} + \mathbf{q} + \mathbf{r}$ and

$$\mathbf{e_i e_i} = \mathbf{e_i^2} = \begin{cases} +\mathbf{1}\ \boldsymbol{for}\ \mathbf{i} = \mathbf{1}, \mathbf{2}, \ldots . , \mathbf{p}-\mathbf{1}, \mathbf{p} \\ -\mathbf{1}\ \boldsymbol{for}\ \mathbf{i} = \mathbf{p}+\mathbf{1}, \ldots \ldots , \mathbf{p}+\mathbf{q} \\ \mathbf{0}\ \ \boldsymbol{for}\ \mathbf{i} = \mathbf{p}+\mathbf{q}+\mathbf{r}, \ldots \ldots . , \mathbf{n} \end{cases} \quad (1)$$

The above-mentioned formulation proves the associativity of linear algebra with identity to define Clifford space $\mathcal{C}\mathbf{l_n}$ of dimension $\mathbf{n} = \mathbf{p} + \mathbf{q} + \mathbf{r}$ generated by the vector space $\mathbb{V}^{\mathbf{n}}$.

© 2026 by the author(s). Distributed under a Creative Commons CC BY license.

Preprints.org (www.preprints.org) | NOT PEER-REVIEWED | Posted: 11 May 2026 doi:10.20944/preprints202605.0666.v1

The basis blades combine to form a generic element called a *multivector* in CA. It is generated as an entity containing several grades of $\mathbf{2^n}$ subspaces in $\mathcal{Cl}_\mathbf{n}$. Such as, $\mathbf{A} = \langle \mathbf{A_0} \rangle + \langle \mathbf{A_1} \rangle + \langle \mathbf{A_2} \rangle + \cdots \ldots . . + \langle \mathbf{A_n} \rangle$ where the multivector $\mathbf{A} \in \mathcal{Cl}_\mathbf{n}$.

The geometric product is expressed for two vectors $\mathbf{a}$ and $\mathbf{b}$ as a combination of the inner and outer products mentioned earlier in this section.

$$\mathbf{ab} = \mathbf{a} \cdot \mathbf{b} + \mathbf{a} \wedge \mathbf{b} \tag{2}$$

B. Two-Dimensional Theory

The elements of the $\mathbf{n}$ dimensional vector space $\mathbb{V}^\mathbf{n}$ are vectors. The higher dimensional oriented subspaces are the basic elements of computation in Clifford Algebra [38]. An extension of the $\mathbf{n}$ dimensional Euclidean vector space $\mathbb{R}$ is represented as $\mathcal{Cl}_\mathbf{n}$. Considering $\mathbf{n} = 2$, the bounded space exists in a plane $\mathbb{R} \times \mathbb{R}$ into linear space $\mathbb{R}^2$. Considering an orthonormal basis $(\mathbf{e_1}, \mathbf{e_2})$ of $\mathbb{R}^2$ having the characteristics of these basis are $\mathbf{e_1}^2 = \mathbf{e_2}^2 = \mathbf{1}$ and $\mathbf{e_{12}} = -\mathbf{e_{21}}$.

Two generic vectors assumed $\mathbf{a}$ and $\mathbf{b}$ of $\mathbb{R}^2$ are stated as linear combinations of the basis elements: $\mathbf{a} = \mathbf{a_1 e_1} + \mathbf{a_2 e_2}$ and $\mathbf{b} = \mathbf{b_1 e_1} + \mathbf{b_2 e_2}$. After multiplication of $\mathbf{a}$ and $\mathbf{b}$, the Clifford product will be

$$\mathbf{ab} = (\mathbf{a_1 e_1} + \mathbf{a_2 e_2})(\mathbf{b_1 e_1} + \mathbf{b_2 e_2})$$

$$= (\mathbf{a_1 b_1} + \mathbf{a_2 b_2}) + (\mathbf{a_1 b_2} - \mathbf{a_2 b_1})\,\mathbf{e_{12}} \tag{3}$$

The product consists of the combination of a scalar and a bivector. A bivector denotes the oriented plane generated by two vectors $\mathbf{a}$ and $\mathbf{b}$. The Clifford product of two vectors of $\mathbb{R}^2$ is expressed as the combination of scalar product (dot product) and wedge product defined in Eq. (2).

It can be concluded by comparing Eq. (2) and Eq. (3).

$$\mathbf{a}.\mathbf{b} = \mathbf{a_1 b_1} + \mathbf{a_2 b_2}$$

$$\mathbf{a} \wedge \mathbf{b} = \begin{vmatrix} \mathbf{a_1} & \mathbf{b_1} \\ \mathbf{a_2} & \mathbf{b_2} \end{vmatrix} \mathbf{e_{12}}$$

The wedge product is known as the outer product, and it is anticommutative, $\mathbf{a} \wedge \mathbf{b} = -\mathbf{b} \wedge \mathbf{a}$. The scalar product is characterized by commutativity, $\mathbf{a}.\mathbf{b} = \mathbf{b}.\mathbf{a}$. In another form (3) can be written as, $\mathbf{ab} = \frac{1}{2}(\mathbf{ab} + \mathbf{ba}) + \frac{1}{2}(\mathbf{ab} - \mathbf{ba})$. So, $\mathbf{a}.\mathbf{b} = \frac{1}{2}(\mathbf{ab} + \mathbf{ba})$ and $\mathbf{a} \wedge \mathbf{b} = \frac{1}{2}(\mathbf{ab} - \mathbf{ba})$.

If $\mathbf{a} \parallel \mathbf{b}$ then $\mathbf{ab} = \mathbf{ba}$, that suggests $\mathbf{a} \wedge \mathbf{b} = \mathbf{0}$, and when $\mathbf{a} \perp \mathbf{b}$ then $\mathbf{ab} = -\mathbf{ba}$, suggesting $\mathbf{a}.\mathbf{b} = \mathbf{0}$.

C. Three-Dimensional Theory

For $\mathbf{n} = \mathbf{3}$, The Euclidean vector space is confined within a linear space $\mathbb{R}^3$. It consists of orthonormal basis of three orthogonal unit vectors $(\mathbf{e_1}, \mathbf{e_2}, \mathbf{e_3})$. Considering two generic vectors $\mathbf{a}$ and $\mathbf{b}$ of $\mathbb{R}^3$ is stated as the linear combinations of the basis elements: $\mathbf{a} = \mathbf{a_1 e_1} + \mathbf{a_2 e_2} + \mathbf{a_3 e_3}$ and $\mathbf{b} = \mathbf{b_1 e_1} + \mathbf{b_2 e_2} + \mathbf{b_3 e_3}$. For $\mathcal{Cl}_3$, the Clifford product between these two vectors $\mathbf{a}$ and $\mathbf{b}$ is,

$$= \sum_{\mathbf{i}=1}^{3} \mathbf{a_i b_i} + \begin{vmatrix} \mathbf{a_1} & \mathbf{b_1} \\ \mathbf{a_2} & \mathbf{b_2} \end{vmatrix} \mathbf{e_{12}} + \begin{vmatrix} \mathbf{a_1} & \mathbf{b_1} \\ \mathbf{a_3} & \mathbf{b_3} \end{vmatrix} \mathbf{e_{13}} + \begin{vmatrix} \mathbf{a_2} & \mathbf{b_2} \\ \mathbf{a_3} & \mathbf{b_3} \end{vmatrix} \mathbf{e_{23}}$$

$$= (\mathbf{a_1 e_1} + \mathbf{a_2 e_2} + \mathbf{a_3 e_3})(\mathbf{b_1 e_1} + \mathbf{b_2 e_2} + \mathbf{b_3 e_3}) \tag{4}$$

It possesses the same properties as the orthonormal basis, $\mathbf{e_1}^2 = \mathbf{e_2}^2 = \mathbf{e_3}^2 = \mathbf{1}$ and $\mathbf{e_{12}} = -\mathbf{e_{21}}, \mathbf{e_{13}} = -\mathbf{e_{31}}, \mathbf{e_{23}} = -\mathbf{e_{32}}$. If three generic vectors $\mathbf{a}$, $\mathbf{b}$, $\mathbf{c}$ are considered, they produce an entry into a new subspace as a trivector element in the Clifford product. A CA space ($\mathcal{Cl}_3$) includes all the subspaces: scalar, vector, bivector, and trivector. Typically, $\mathbf{e_{123}}$ **denotes** the oriented volume element in $\mathbb{R}^3$ referred to as a trivector.

© 2026 by the author(s). Distributed under a Creative Commons CC BY license.

Preprints.org (www.preprints.org) | NOT PEER-REVIEWED | Posted: 11 May 2026 doi:10.20944/preprints202605.0666.v1

D. Multivector Approach in 2𝔻 and 3𝔻

A multivector is defined as the collection of heterogeneous elements over CA space $\mathcal{Cl}_n$. Scalar, vector, bivector and trivector are the oriented subspaces as elements of a multivector in $\mathcal{Cl}_3$ space. The general concept is 2^n number of elements or subspaces are possible for n-dimensional space. The generic element or multivector is a linear combination of the 2^n basis elements with real coefficients. In case of $n = 3$, $\mathcal{Cl}_3$ space consists of 2^3 elements.

A multivector consists of various subspaces within it. Each of these subspaces is referred to as a blade. A Euclidean vector space $\mathbb{R}^2$ contains the orthonormal basis is (e_1,e_2). The elements are 1 (scalar), e_1,e_2 (vector), e_{12} (bivector) form a basis $(1, e_1, e_2, e_{12})$ for the Clifford Algebra space $\mathcal{Cl}_2$ of $\mathbb{R}^2$. Therefore, the basic multivector for $\mathcal{Cl}_2$ is,

$$a = a_0 + a_1e_1 + a_2e_2 + a_{12}e_{12} \tag{5}$$

The pseudoscalar component I in $\mathcal{Cl}_2$ is the bivector subspace. The subspace e_{12} is squared to give $I^2 = -1$ according to the identity mentioned above. This characteristic is derived from complex numbers where an imaginary plane is present to find $\sqrt{-1}$ [39]. The multivector in Eq. (5) is rewritten as

$$a = a_0 + a_1e_1 + a_2e_2 + a_{12}I \tag{6}$$

According to the theory of multivector, the above-said Eq. (5) can be written as

$$a = \langle a_0 \rangle + \langle a_1 \rangle + \langle a_2 \rangle \tag{7}$$

Eq. (7) describes a component acquired by including basis vectors of $\mathbb{R}^2$ and it is a multivector in $\mathcal{Cl}_2$.

Similarly, for Clifford's Algebra space $\mathcal{Cl}_3$, the general form of multivector is written as

$$a = a_0 + \sum_{i=1}^{3} a_ie_i + a_{12}e_{12} + a_{13}e_{13} + a_{23}e_{23} + a_{123}e_{123} \tag{8}$$

For $\mathcal{Cl}_3$, the multivector is now expressed as

$$a = \langle a_0 \rangle + \langle a_1 \rangle + \langle a_2 \rangle + \langle a_3 \rangle \tag{9}$$

E. Reflection in Clifford Space

The rationale for CA's acceptance is the representational capability of its operators. Geometric transformations such as reflection and rotation in CA space can be formulated as algebraic operators.

The reflected part of vector x concerning a fixed vector a is axa^{-1} illustrated in Figure 2. When a plane is perpendicular to a then the reflected component will be $-axa^{-1}$. In simpler term, a blade X is mirrored concerning the vector a. It forms a vector X' by using a formula $X' \mapsto aXa^{-1}$. X' is the reflection of X in vector a.

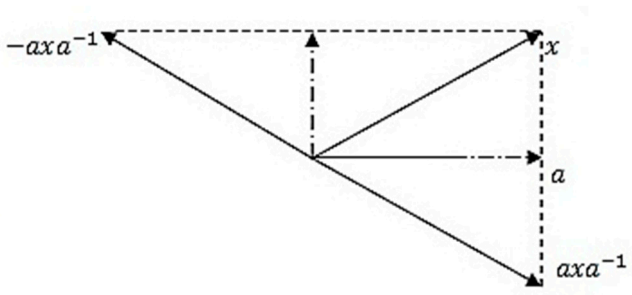

Figure 2. Reflection of a vector.

F. Rotation in Clifford Space

© 2026 by the author(s). Distributed under a Creative Commons CC BY license.

Preprints.org (www.preprints.org) | NOT PEER-REVIEWED | Posted: 11 May 2026 doi:10.20944/preprints202605.0666.v1

Rotation is denoted by a pair of reflections. Two consecutive reflections of a vector cause that vector to rotate by a specific angle. In Figure 3, $\boldsymbol{a}$ and $\boldsymbol{b}$ are the unit vectors that are angled at $\boldsymbol{\varphi}$. It aims to rotate a vector $\boldsymbol{x}$ to $\boldsymbol{x}$". The vector $\boldsymbol{x}$ makes an angle $\boldsymbol{\theta_1}$ with $\boldsymbol{a}$ where $\boldsymbol{\theta_1 < \varphi}$. After reflection through angle $\boldsymbol{\theta_1}$, $\boldsymbol{x}$ becomes $\boldsymbol{x}'$.

The angle between vector $\boldsymbol{x}'$ to vector $\boldsymbol{b}$ is $(\boldsymbol{\varphi + \theta_1})$ for the second reflection. Therefore, after reflection through $(\boldsymbol{\varphi + \theta_1})$, the vector $\boldsymbol{x}'$ becomes the rotated vector $\boldsymbol{x}$".

Mathematically, the two reflections are described by, $\boldsymbol{x' = axa^{-1}}$ and $\boldsymbol{x" = bx'b^{-1}}$. In simpler form, the rotated vector

$$\begin{aligned} \boldsymbol{x"} &= \boldsymbol{b(axa^{-1})\, b^{-1}} \\ &= \boldsymbol{b(a^{-1}xa)b^{-1} = (ba^{-1})x(ab^{-1})} \\ &= \boldsymbol{RxR^{-1}} \text{ where } \boldsymbol{RR^{-1} = 1}. \end{aligned}$$

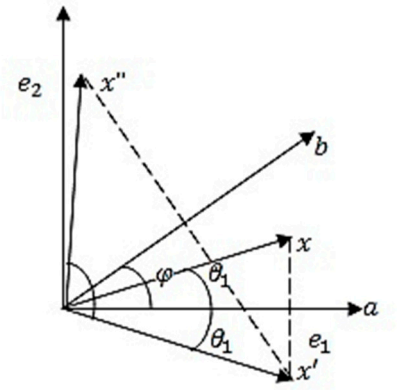

Figure 3. Rotation of a vector.

Here $\mathbf{R}$ indicates a multivector, which is also referred to as a Rotational operator or Rotor. If a rotation operation is occured by an angle $\boldsymbol{\varphi}$ around the origin, then $\mathbf{R = \cos\varphi + I\sin\varphi}$. $\mathbf{I}$ is the pseudoscalar for the corresponding CA space. It can be written as $\mathbf{R = e^{I\varphi}}$ and $\mathbf{R^{-1} = e^{-I\varphi}}$.

In the standard representation of rotation in higher dimensional subspaces, a rotor is employed for an arbitrary blade through this equation is

$$\mathbf{X \longmapsto RXR^{-1}} \tag{10}$$

The reflection and rotation functions in CA enhance its ability to represent any geometric shapes. These two functions are utilized for geometric transformations of any subspace within Clifford space. Generally, a $\mathbf{Grade - k}$ $(\mathcal{G}_\mathbf{k})$ vector $\mathbf{X}$ in $\mathcal{C}\mathbf{l}_3$ is reflected in a plane perpendicular to a $\mathcal{G}_\mathbf{k}$ vector $\mathbf{n}$ is $-(-\mathbf{1})^\mathbf{k}\mathbf{nXn^{-1}}$ as transformed $\mathcal{G}_\mathbf{k}$ vector $\mathbf{X}'$ where $\mathbf{0 \le k \le 3}$. A rotation is characterized as two sequential reflections. The reflection $\mathbf{-nXn^{-1}}$ followed by another reflection in a plane perpendicular to a $\mathcal{G}_1$ vector $\mathbf{m}$ results in another $\mathcal{G}_\mathbf{k}$ vector in the form of $\mathbf{(mn)B(nm)}$. The product $\mathbf{mn}$ characterizes a multivector and is considered a rotational component or *Rotor* $\mathbf{R}$. The revised form of rotation is formulated as $\mathbf{R\tilde{X}\tilde{R}}$ where $\mathbf{R\tilde{R} = 1}$ and $\tilde{\mathbf{R}}$ represents the reverse of the Rotor $\mathbf{R}$.

4. Clifford Color Space

The RGB color model corresponds to a $\mathbf{3}\mathbb{D}$ Euclidean space. Each pixel in an image is characterized by a triplet consisting of red, green, and blue components. Each color functions as a vector, with the $\mathbf{x}$-axis representing the red component, the $\mathbf{y}$-axis indicating green, and the $\mathbf{z}$-axis delineating blue, respectively. It is noted that eight distinct colors can be rendered based on the RGB components illustrated below in Figure 4.

© 2026 by the author(s). Distributed under a Creative Commons CC BY license.

Preprints.org (www.preprints.org) | NOT PEER-REVIEWED | Posted: 11 May 2026 doi:10.20944/preprints202605.0666.v1

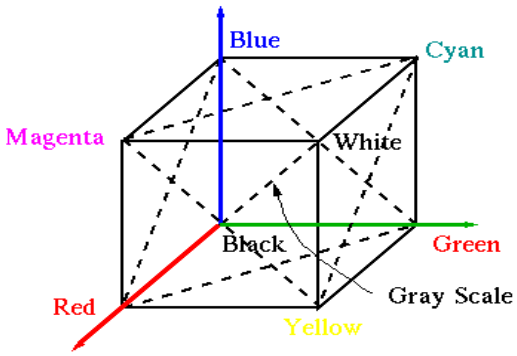

Figure 4. RGB Color Model.

According to the Venn diagram in Figure 5 of the RGB color model, the colors include Black, Red, Green, Blue, Yellow, Magenta, Cyan, and White. The intersection of R, G, and B produces Cyan, Magenta, and Yellow, respectively. The center of all intersections represents white. The area outside the red, green, and blue set is regarded as Black.

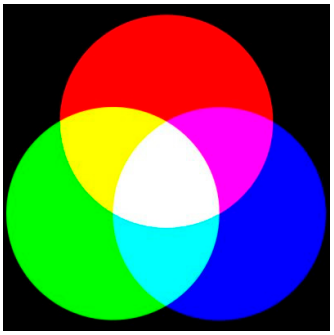

Figure 5. Venn Diagram representation of RGB Color Model.

Every pixel of an image is depicted by a $\mathbf{3}\mathbb{D}$ Euclidean color space. In $\mathbb{R}^{\mathbf{3}}$ the orthonormal basis is $\mathbf{e_1}$, $\mathbf{e_2}$ and $\mathbf{e_3}$ symbolizing red, green, and blue components, respectively. So, the real value of RGB will be related with this orthonormal basis to produce a homogeneous vector. Assume, for a pixel. $(\mathbf{x}, \mathbf{y})$ the vector

$$\mathbf{col}(\mathbf{x}, \mathbf{y}) = \mathbf{r}(\mathbf{x}, \mathbf{y})\mathbf{e_1} + \mathbf{g}(\mathbf{x}, \mathbf{y})\mathbf{e_2} + \mathbf{b}(\mathbf{x}, \mathbf{y})\mathbf{e_3} \quad (11)$$

where $\mathbf{r}(\mathbf{x}, \mathbf{y})$, $\mathbf{g}(\mathbf{x}, \mathbf{y})$ and $\mathbf{b}(\mathbf{x}, \mathbf{y})$ are RGB real values at pixel $(\mathbf{x}, \mathbf{y})$. Therefore, for an image having $\mathbf{M} \times \mathbf{N}$ pixels, the function will be,

$$\mathbf{col^{MN}}(\,) = \sum_{\mathbf{x=0}}^{\mathbf{M-1}} \sum_{\mathbf{y=0}}^{\mathbf{N-1}} \mathbf{r}(\mathbf{x}, \mathbf{y})\mathbf{e_1} + \mathbf{g}(\mathbf{x}, \mathbf{y})\mathbf{e_2} + \mathbf{b}(\mathbf{x}, \mathbf{y})\mathbf{e_3} \quad (12)$$

According to Eq. (11), there will be $\mathbf{M} \times \mathbf{N}$ number of homogenous vectors for each of the pixels in an image.

The bivector basis is utlized to depict a color for $\mathbb{R}^{\mathbf{3}}$ in relation to a pixel [7]. The color vector is written as

$$\mathbf{col_{m,n}} = \mathbf{r_{m,n}}\mathbf{e_{23}} + \mathbf{g_{m,n}}\mathbf{e_{31}} + \mathbf{b_{m,n}}\mathbf{e_{12}} \quad (13)$$

It has been noted that a pixel's color is depicted by a pure quaternion [40]. The above function follows the quaternionic concept because each of the $\mathbf{e_{ij}}^{\mathbf{2}} = -\mathbf{1}$.

A. Color Image

The color model offers a $\mathbf{3}\mathbb{D}$ Euclidean space is mentioned in earlier section. RGB color spaces are the oriented subspaces in $\mathbf{3}\mathbb{D}$ CA ($\mathcal{C}\mathbf{l_3}$). For $\mathcal{C}\mathbf{l_3}$ space there would be $\mathbf{2^3}$(eight) numbers of subspaces possible. Therefore, it identifies Black as the scalar, (Red, Green, Blue) as the vector, (Cyan,

© 2026 by the author(s). Distributed under a Creative Commons CC BY license.

Preprints.org (www.preprints.org) | NOT PEER-REVIEWED | Posted: 11 May 2026 doi:10.20944/preprints202605.0666.v1

Magenta, Yellow) as the bivector, and White as the trivector. The bivector arises from Cyan being produced by the blue and green components at their peak magnitude. This signifies that Cyan exists within the plane formed by the blue and green vectors. In $\mathcal{C}\mathbf{l}_3$, any plane formed by the vectors is a bivector. Likewise, Magenta and Yellow are the bivectors corresponding to Red-Blue and Red-Green. Black does not contain any of the RGB components considered as a scalar. White serves as the volume element in $\mathcal{C}\mathbf{l}_3$; since each vector has its maximum magnitude, white is regarded as the trivector. As CA possesses coordinate-free properties, it is utilized to represent each color with a multivector. One of the subspaces within the multivector is responsible for defining a color. In this proposal, the RGB color model is substituted with $\mathcal{C}\mathbf{l}_3$ space because it includes scalar, vector, bivector, and trivector rather than a homogeneous vector. A multivector is introduced to represent a single pixel, incorporating all potential dimensional grades. Say, at pixel (x, y) the multivector:

$$\mathbf{col}(\mathbf{x},\mathbf{y}) = \mathbf{P} + \mathbf{r}(\mathbf{x},\mathbf{y})\mathbf{e_r} + \mathbf{g}(\mathbf{x},\mathbf{y})\mathbf{e_g} + \mathbf{b}(\mathbf{x},\mathbf{y})\mathbf{e_b} + \boldsymbol{\alpha}\mathbf{e_{rg}} + \boldsymbol{\beta}\mathbf{e_{gb}} + \boldsymbol{\gamma}\mathbf{e_{rb}} + \mathbf{Q}\mathbf{e_{rgb}} \quad (14)$$

where $\mathbf{P}$ as Black where no RGB component exists, i.e., no vector component is present in this color definition. $\mathbf{Q}$ acts as white consisting the maximum magnitude of Red, Green, and Blue, defined as the volume element $\mathbf{e_{rgb}}$. And $\boldsymbol{\alpha}$, $\boldsymbol{\beta}$, γ are the real values linked with the bivectors. $\mathbf{e_{rg}}$, $\mathbf{e_{gb}}$ & $\mathbf{e_{rb}}$ bivectors represent the plane Red-Green, Green-Blue, and Red-Blue, respectively. Therefore the wedge product is the representation of color. Color blade is a $\mathbf{Grade} - \mathbf{1}$ multivector when $\mathbf{e_r}$, $\mathbf{e_g}$ & $\mathbf{e_b}$ is not null, and the real values are less than maximum values but not zero. However, it is also accurate that the bivector signifies a color when one component is absent. Assuming for a pixel $(\mathbf{x},\mathbf{y})$ there is no blue component, $\boldsymbol{\alpha}\mathbf{e_{rg}} = \mathbf{r}(\mathbf{x},\mathbf{y})\mathbf{e_r} \wedge \mathbf{g}(\mathbf{x},\mathbf{y})\mathbf{e_g}$. If a pixel $(\mathbf{x},\mathbf{y})$ gives **(255,255,0)** then $\boldsymbol{\alpha}$ reflects yellow color and $\mathbf{e_{rg}}$ suggests the subspace in which yellow color belongs. Cyan & Magenta colors are generated in similar way. To depict white color, a trivector is required as it comprises RGB elements at their maximum intensity at pixel $(\mathbf{x},\mathbf{y})$, thus

$$\mathbf{Q}\mathbf{e_{rgb}} = \mathbf{r}(\mathbf{x},\mathbf{y})\mathbf{e_r} \wedge \mathbf{g}(\mathbf{x},\mathbf{y})\mathbf{e_g} \wedge \mathbf{b}(\mathbf{x},\mathbf{y})\mathbf{e_b} \quad (15)$$

This function proposed in Eq. (14) is applicable for all the $\mathbf{2^{24}}$ colors possible for this color model. Therefore, for an image having $\mathbf{M} \times \mathbf{N}$ pixels, the function will be

$$\mathbf{col^{MN}}(\mathbf{x},\mathbf{y}) = \sum_{\mathbf{x=0}}^{\mathbf{M-1}} \sum_{\mathbf{y=0}}^{\mathbf{N-1}} \mathbf{P} + \mathbf{r}(\mathbf{x},\mathbf{y})\mathbf{e_r} + \mathbf{g}(\mathbf{x},\mathbf{y})\mathbf{e_g} + \mathbf{b}(\mathbf{x},\mathbf{y})\mathbf{e_b} + \boldsymbol{\alpha}\mathbf{e_{rg}} + \boldsymbol{\beta}\mathbf{e_{gb}} + \boldsymbol{\gamma}\mathbf{e_{rb}} + \mathbf{Q}\mathbf{e_{rgb}} \quad (16)$$

It indicates the typical structure of a function represented as a multivector in $\mathcal{C}\mathbf{l}_3$ space. The preceding Eq. (16) illustrates a multivector that serves to represent an image on a pixel-by-pixel basis. Various shades of red, green, and blue are utilized in an image. Within those shades it is feasible that at any pixel $(\mathbf{x},\mathbf{y})$, one or more RGB components may be absent. For no RGB components, the function is $\mathbf{col}(\mathbf{x},\mathbf{y}) = \mathbf{P}$, i.e., the color is black. Another case may occur where no Red component is present, then $\mathbf{col}(\mathbf{x},\mathbf{y}) = \boldsymbol{\beta}\mathbf{e_{gb}}$. It is observed that Eq. (14) can be signified as minimum by one term and maximum by three terms. The multivector behaves like any of the $\mathbf{Grade} - \mathbf{k}$ vector from CA perception. In $\mathcal{C}\mathbf{l}_3$ space, say for Black $\mathbf{Grade} - \mathbf{0}$ (scalar), for Yellow $\mathbf{Grade} - \mathbf{2}$ (bivector) is the behavior of multivector. So, based on the proposal the color blades are created in $\mathcal{C}\mathbf{l}_3$ space. These color blades serve to signify a color.

B. Grayscale Image

The gray value of a pixel in a color image is computed by a function known as the intensity function, shown in Figure 6 below. The gray value determines the pixel's intensity. The function is dependent on the RGB component at a pixel $(\mathbf{x},\mathbf{y})$ of an image. It is defined as

$$\mathcal{G}(\mathbf{x},\mathbf{y}) = \mathbf{r}(\mathbf{x},\mathbf{y}) + \mathbf{g}(\mathbf{x},\mathbf{y}) + \mathbf{b}(\mathbf{x},\mathbf{y}) \quad (17)$$

The gray value for a certain pixel in an image is expressed as a vector. The color vector stated in Eq. (11) is combined with the intensity function described in Eq. (17) to derive a grayscale vector. It is defined as $\mathcal{G}(\mathbf{x},\mathbf{y})$ at a pixel $(\mathbf{x},\mathbf{y})$ and is shown in Eq. (18).

$$\mathcal{G}(\mathbf{x},\mathbf{y}) = \mathbf{0.3}\,\mathbf{r}(\mathbf{x},\mathbf{y})\mathbf{e_1} + \mathbf{0.59}\mathbf{g}(\mathbf{x},\mathbf{y})\mathbf{e_2} + \mathbf{0.11}\mathbf{b}(\mathbf{x},\mathbf{y})\mathbf{e_3} \quad (18)$$

© 2026 by the author(s). Distributed under a Creative Commons CC BY license.

Preprints.org (www.preprints.org) | NOT PEER-REVIEWED | Posted: 11 May 2026 doi:10.20944/preprints202605.0666.v1

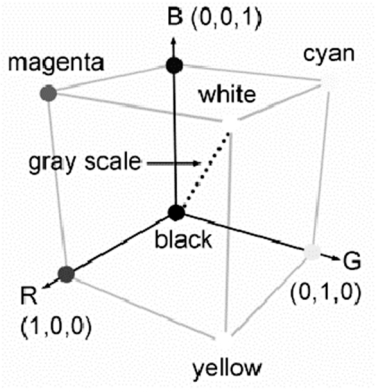

Figure 6. RGB Color Model with Grayscale Labelling.

The gray value of a pixel is computed with the help of an RGB component in $\mathcal{C}\mathbf{l}_3$ space. Though this value reflects the intensity or scalar value, it is represented in terms of homogeneous vectors according to Eq. (18). A grayscale image is represented as a particular form of vectors in $\mathcal{C}\mathbf{l}_3$ space. A grayscale vector is defined as the segment of a volume element $\mathbf{e}_{\mathbf{rgb}}$ in $\mathcal{C}\mathbf{l}_3$ space. Therefore, Eq. (18) is rewritten as;

$$\mathcal{G}(\mathbf{x},\mathbf{y}) = \left(\mathbf{0.3}\boldsymbol{\alpha}\mathbf{e}_{\mathbf{r}}(\mathbf{x},\mathbf{y}) + \mathbf{0.59}\boldsymbol{\beta}\mathbf{e}_{\mathbf{g}}(\mathbf{x},\mathbf{y}) + \mathbf{0.11}\boldsymbol{\gamma}\mathbf{e}_{\mathbf{b}}(\mathbf{x},\mathbf{y})\right)\mathbf{e}_{\mathbf{rgb}}(\mathbf{x},\mathbf{y}) \quad (19)$$

It describes the nature of the grayscale vector as a segment. The segmented vector in Eq. (20) is transformed into a bivector.

$$\mathcal{G}(\mathbf{x},\mathbf{y}) = \mathbf{0.3}\boldsymbol{\alpha}\mathbf{e}_{\mathbf{gb}}(\mathbf{x},\mathbf{y}) + \mathbf{0.59}\boldsymbol{\beta}\mathbf{e}_{\mathbf{br}}(\mathbf{x},\mathbf{y}) + \mathbf{0.11}\boldsymbol{\gamma}\mathbf{e}_{\mathbf{gr}}(\mathbf{x},\mathbf{y}) \quad (20)$$

A combination of three-color planes in $\mathcal{C}\mathbf{l}_3$ space as a summation of a bivector represents a gray value for a certain pixel $(\mathbf{x},\mathbf{y})$. Therefore, for a grayscale image having $\mathbf{M}\times\mathbf{N}$ pixels, the function will be

$$\mathcal{G}^{\mathbf{MN}}(\mathbf{x},\mathbf{y}) = \sum_{\mathbf{x}=\mathbf{0}}^{\mathbf{M}-\mathbf{1}}\sum_{\mathbf{y}=\mathbf{0}}^{\mathbf{N}-\mathbf{1}}\mathbf{0.3}\boldsymbol{\alpha}\mathbf{e}_{\mathbf{gb}}(\mathbf{x},\mathbf{y}) + \mathbf{0.59}\boldsymbol{\beta}\mathbf{e}_{\mathbf{br}}(\mathbf{x},\mathbf{y}) + \mathbf{0.11}\boldsymbol{\gamma}\mathbf{e}_{\mathbf{gr}}(\mathbf{x},\mathbf{y}) \quad (21)$$

The general form of multivector for gray value at a certain pixel is derived as,

$$\mathcal{G}_{\mathbf{gray}} = \boldsymbol{\alpha}\mathbf{e}_{\mathbf{gb}} + \boldsymbol{\beta}\mathbf{e}_{\mathbf{br}} + \boldsymbol{\gamma}\mathbf{e}_{\mathbf{gr}} \quad (22)$$

A vector $\mathbf{v}$ is the grayscale vector pointing towards the volume element in RGB color space. The segmented part $\mathbf{v}$ is perpendicular to the three planes holding RGB values of $(\boldsymbol{\alpha},\boldsymbol{\beta},\ \boldsymbol{\gamma})$. Every perpendicular to the respective plane is generating a bivector with respect to $\mathbf{v}$ shown in Figure 7.

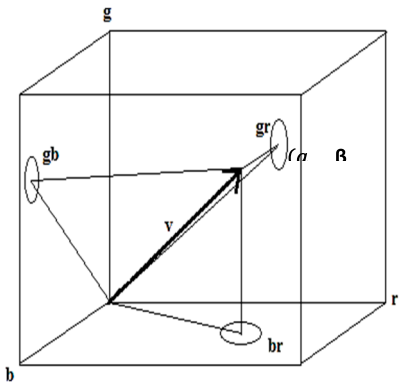

Figure 7. Representation of the grayscale multivector.

5. Retinal Fundus Image Representation

© 2026 by the author(s). Distributed under a Creative Commons CC BY license.

Preprints.org (www.preprints.org) | NOT PEER-REVIEWED | Posted: 11 May 2026 doi:10.20944/preprints202605.0666.v1

The RGB color cube forms a $\mathbb{3D}$ Euclidean space. Any color in this space is defined as a vector. Clifford Algebra defines each color as a color multivector, as discussed in [4]. The colors of each pixel are mapped from Clifford's color space, which is mentioned in the earlier section. Any color in the retinal fundus image is defined as a multivector or $\mathbf{Grade} - \mathbf{k}$ vector, and after rotation of that vector, a new color is formed. The substitute color may contain new features to help further preprocess the image. Therefore, a retinal fundus image having $\mathbf{M} \times \mathbf{N}$ pixels following Eq. (16) is

$$\mathbf{RFI^{MN}(x,y)} = \sum_{\mathbf{x=0}}^{\mathbf{M-1}} \sum_{\mathbf{y=0}}^{\mathbf{N-1}} \mathbf{P} + \mathbf{r(x,y)e_r} + \mathbf{g(x,y)e_g} + \mathbf{b(x,y)e_b} + \boldsymbol{\alpha}\mathbf{e_{rg}} + \boldsymbol{\beta}\mathbf{e_{gb}} + \boldsymbol{\gamma}\mathbf{e_{rb}} + \mathbf{Qe_{rgb}} \quad (23)$$

A color blade is the subspace or $\mathbf{Grade} - \mathbf{k}$ vector in $\mathcal{C}\mathbf{l_3}$. The function in Eq. (23) shows how the multivectors completely define a retinal image. In contrast with the quaternion approach [7], this proposal does not limit the colors among the bivector basis. Every subspace will be responsible for defining a color, not only the bivectors. Each color against each pixel in the images must have different bivector definitions.

In many cases, the colors are defined by vectors indicating avoidance to represent the colors by bivector. Higher dimensional subspace rotations are always complicated and computationally costly when considering the fundus images. To avoid that complication and reduce the computational time, minimizing the number of bivectors with a generalized multivector representing the images is necessary. This is the real cause for representing the retinal fundus images by $\mathbf{Grade} - \mathbf{k}$ vectors of multivectors.

The methodology is discussed in two steps procedure. Initially, the image pixels are converted to Clifford color space. In the next step, the rotor operator is applied to realize the multivector representation of the fundus image shown in Figures 8 and 9, respectively.

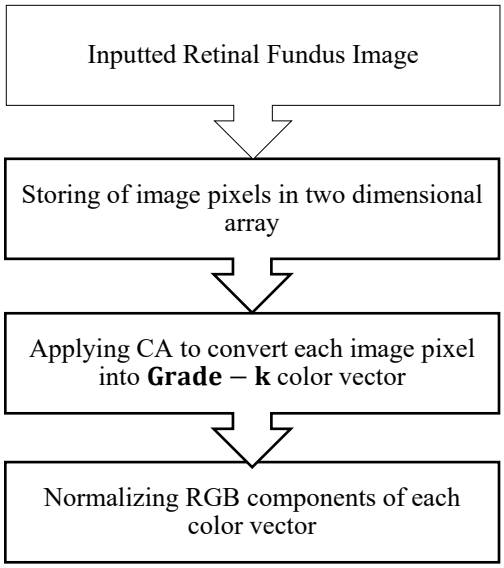

Figure 8. Conversion to Clifford color space.

© 2026 by the author(s). Distributed under a Creative Commons CC BY license.

Preprints.org (www.preprints.org) | NOT PEER-REVIEWED | Posted: 11 May 2026 doi:10.20944/preprints202605.0666.v1

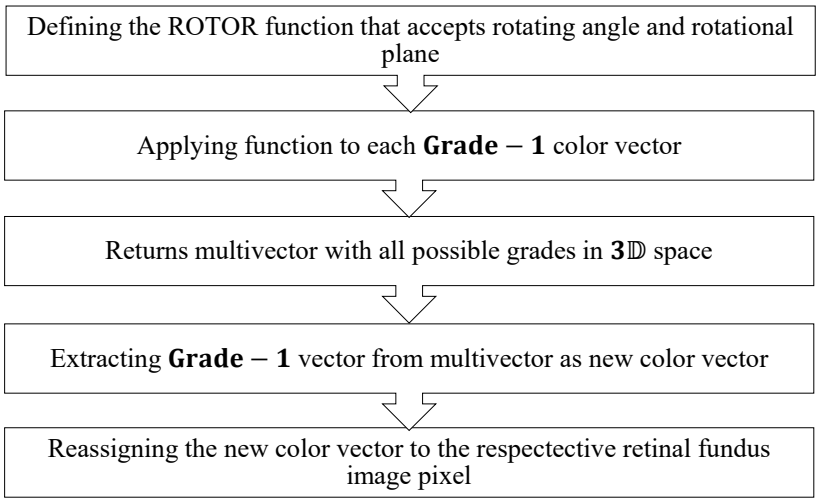

Figure 9. Impact of rotation operation in Clifford space.

A. Conversion to Clifford Color Space

The process begins with the input of a raw retinal fundus image. While considering the image data structure, the image is converted into a two-dimensional array format for computational efficiency and manipulation. An element in the array represents each pixel in the image. Each pixel in the image is transformed into a $\mathbf{Grade} - \mathbf{k}$ vector using CA.

The process begins with the input of a raw retinal fundus image. While considering the image data structure, the image is converted into a two-dimensional array format for computational efficiency and manipulation. An element in the array represents each pixel in the image. Each pixel in the image is transformed into a $\mathbf{Grade} - \mathbf{k}$ vector using CA. This allows the fundus image to be mapped into $\mathcal{C}\mathbf{l}_3$ Clifford color space. This representation aims to capture more complex color and spatial information than traditional RGB representation. The RGB components of each color vector transformed into multivector elements are normalized to ensure data consistency and improve subsequent processing steps. This preprocessing pipeline prepares the retinal fundus image for further CA operation.

B. Impact of Rotational Operation on Clifford Color Space

CA framework operated on individual color vectors as multivectors, allowing the technique to control color transformations precisely. A new function has been proposed based on the rotor operator. This function serves as the core of the color manipulation process. Defining the transformation requires a rotation angle and a subspace as input. The rotor is applied to each color $\mathbf{Grade} - \mathbf{k}$ vector, resulting in a multivector and encapsulating the rotated color data in a higher-dimensional space. The desire $\mathbf{Grade} - \mathbf{1}$ color vector is fetched from the multivector. Preserving the required color features is essential while introducing the desired modifications. The modified color $\mathbf{Grade} - \mathbf{k}$ vectors are reinstated into the image, creating an alternative version of the original retinal fundus image. The rotating angle and subspace have a pivotal role in these changes. This approach provides flexibility in adjusting color and brightness characteristics while maintaining the underlying retinal image structure. It is possible to optimize image quality by carefully selecting the rotation angle and plane.

The rotor as function $\mathcal{R}$, which accepts the angle of rotation $\boldsymbol{rot_\theta}$ and rotational subspace $\boldsymbol{rot_P}$ is defined in Eq. (24). The rotational subspace is the axis that helps to rotate the whole Clifford color space for the entire image.

$$\mathcal{R}(\boldsymbol{rot_\theta}, \boldsymbol{rot_P}) = \boldsymbol{e^{-P\theta/2}} \tag{24}$$

The rotor operator considers $\mathbf{Grade} - \mathbf{k}$ vector as a plane. The function, as mentioned earlier, defines the rotation operation of any $\mathbf{Grade} - \mathbf{k}$ vector along any $\boldsymbol{P}$ plane with $\boldsymbol{\theta}$ angle. CA

© 2026 by the author(s). Distributed under a Creative Commons CC BY license.

Preprints.org (www.preprints.org) | NOT PEER-REVIEWED | Posted: 11 May 2026 doi:10.20944/preprints202605.0666.v1

permits straightforward generalization to the rotation of $\mathbf{3}\mathbb{D}$ subspaces. A rotor can be applied immediately to an arbitrary $\mathbf{Grade} - \mathbf{k}$ vector $\mathbf{X}$ through the Eq. (25) mentioned in [4].

$$\mathbf{X_{rot}} \mapsto \boldsymbol{\mathcal{R}}\,\mathbf{X}\,\boldsymbol{\mathcal{R}}^{-1} \tag{25}$$

The depiction of the input and outputs are carried out pictorially in Figures 10, 11, 12 & 13. Human interpretable retinal fundus image figures will play a key role in perceptual observation. The color layer in both input and output images helps to differentiate the before-after effect. However, representing similar input-output cases (which may occur in a few) may require an RGB plot showing multivector orientation in Clifford space and an RGB histogram version. The pattern or structure of the $\mathbf{Grade} - \mathbf{k}$ scatter plot facilitates the discrimination of the orientation changes. From the view of the machine, the depiction of the plot is the best way of understanding the entire image for the color element. Another representation technique is the histogram of RGB components, which checks the argument prepared in the procedure. It also assists in making a correct and rational conclusion that further improves the decision-making process for subsequent analysis.

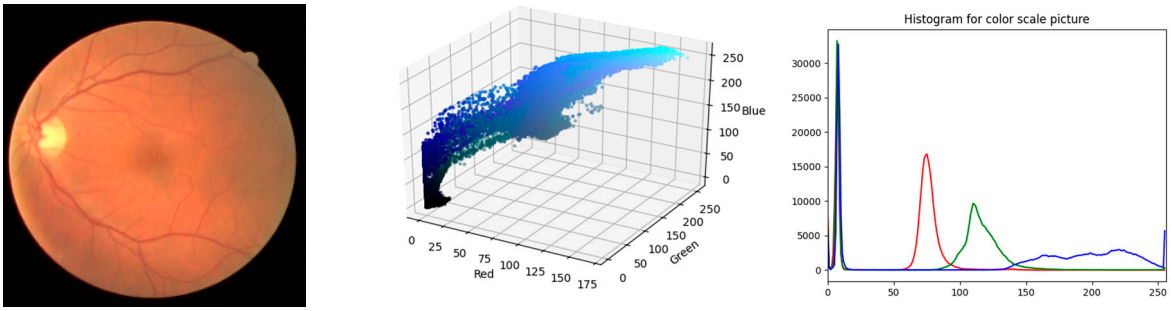

(a) (b) (c)

Figure 10. (a) Inputted fundus image (b) RGB scatter plot (c) RGB color Histogram.

rot_P / rot_θ	e_{12}	e_{23}	e_{13}
$\frac{\pi}{2}$	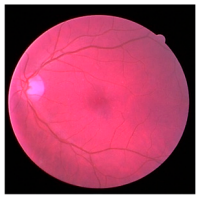		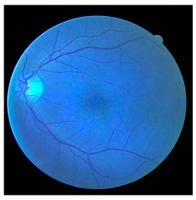
$\frac{\pi}{3}$	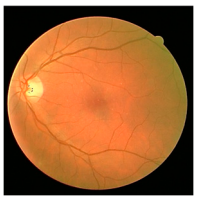	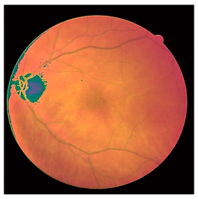	
$\frac{\pi}{4}$	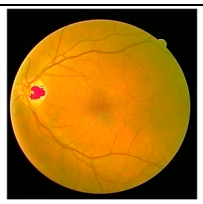	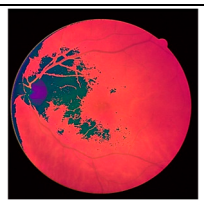	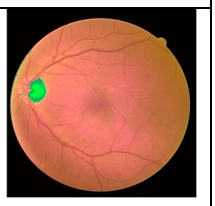

Figure 11. Rotored retinal fundus image in different plane & rotating angle.

© 2026 by the author(s). Distributed under a Creative Commons CC BY license.

Preprints.org (www.preprints.org) | NOT PEER-REVIEWED | Posted: 11 May 2026 doi:10.20944/preprints202605.0666.v1

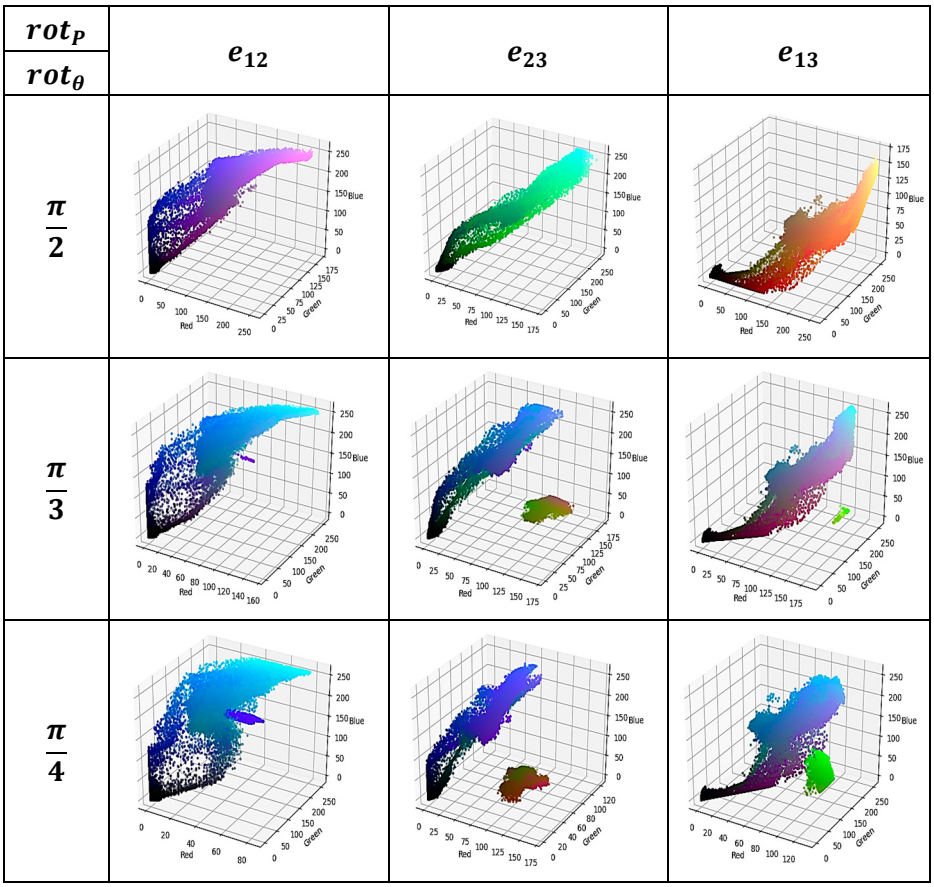

Figure 12. Rotored image RGB scatter plot in different planes and rotation.

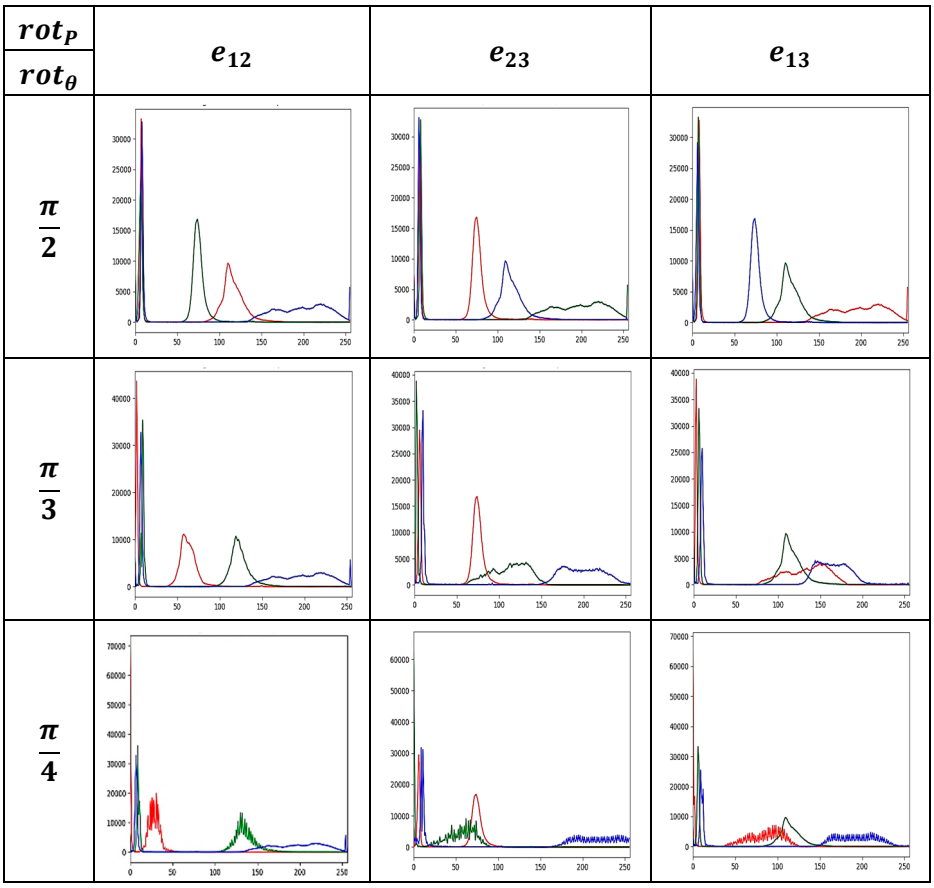

Figure 13. Rotored image color histogram in different planes and rotation.

© 2026 by the author(s). Distributed under a Creative Commons CC BY license.

Preprints.org (www.preprints.org) | NOT PEER-REVIEWED | Posted: 11 May 2026 doi:10.20944/preprints202605.0666.v1

C. Post Rotation Effects in Image Representation

Initially, three types of rotational angle $(\boldsymbol{rot_\theta})$ – $\frac{\pi}{2}, \frac{\pi}{3}, \frac{\pi}{4}$ is considered along with three different bivector planes $\boldsymbol{(rot_P)}$ - $\boldsymbol{e_{12}, e_{23}, e_{13}}$, to realize the multivector color orientation in Clifford's color space. The changes after applying the rotor function are depicted in Figures 11, 12 & 13 below.

The pseudoscalar plane $(\mathbf{e_{123}})$ generally represents the whole $\mathbf{3}\mathbb{D}$ space of RGB component vectors. It is defined as a volume rather than a plane due to its highest grade as a vector in a multivector. Any vector is expected to rotate in a volume, interpreting the rotation of the whole space or volume. That doesn't help to create any rotational movement of the individual vector with respect to the space. The main schema of the rotation of vectors with the help of the rotor operator is the alteration of colors in the retinal fundus image. It is observed that no such minor changes occurred in the color representation of the fundus images. The rotation on pseudoscalar $\mathbf{e_{123}}$ is actually the rotation of the whole Clifford space. This is the highest dimension of the space carrying all $\mathbf{Grade - k}$ vectors except itself. This establishes the claim of rotation of the color space or volume for $\mathbf{3}\mathbb{D}$ space. Hence, no changes had been observed for any rotational angle under these circumstances. The rotor function mentioned above has no impact on this pseudoscalar axis.

D. Analysis of Image Representation

This study focuses on a specific rotation angle, $\frac{\pi}{2}$, for color analysis in retinal images. Ophthalmologists found that this angle significantly impacts color vector transformations, leading to a more uniform color distribution across the image. In contrast, other rotation angles caused color variations, particularly in brighter image regions. The study emphasizes the importance of angle. $\frac{\pi}{2}$, in redirecting all original image colors towards specific color channels for different bivector axes, suggesting its potential for enhancing image contrast and color representation.

Figure 14 illustrates the transformation of the retinal fundus images in three suggested planes with respect to $\mathbf{3}\mathbb{D}$ Clifford color space. The components are treated as unit vectors in the space. The vectors $\mathbf{e_1}, \mathbf{e_2}, \mathbf{e_3}$ are Red, Green, and Blue components, respectively. The input fundus image is transformed into the corresponding Magenta channel image when each color vector is rotated at $\boldsymbol{e_{12}}$ - plane for $\frac{\pi}{2}$. Similarly, a Yellow mix green channel image is generated for $\frac{\pi}{2}$ rotation at $\boldsymbol{e_{23}}$ - plane. In the third development, a Cyan-based image is formed for $\frac{\pi}{2}$ rotation at $\boldsymbol{e_{13}}$ - plane.

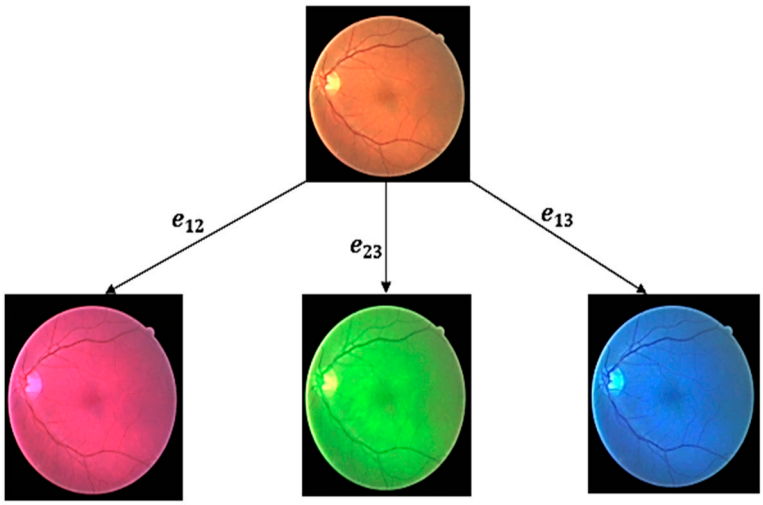

Figure 14. Ophthalmologist interpretable figure for $\mathbf{90°}$ rotation.

The above points apply to combinations of dominant color channels. There will always be a color modification or distortion probability if the other rotating angles are monitored on the color vectors.

© 2026 by the author(s). Distributed under a Creative Commons CC BY license.

Preprints.org (www.preprints.org) | NOT PEER-REVIEWED | Posted: 11 May 2026 doi:10.20944/preprints202605.0666.v1

Often, the RFI gets skewed when working with a rotation of 45° or 60°. The proper rotational angle provides the correct phase toward preprocessing, such as enhancement and denoising.

While considering the color multivector orientation, a scatter plot is an excellent tool for comparing pairs of values to see if they are related. Researchers frequently use scatter plots. It is deducing the magnitude of the vector components for a color in the $\mathbb{3D}$ Clifford space. The color $\mathbf{Grade} - \mathbf{k}$ vector at the plot determines the pixel's color. The plot describes the orientation of the color component in the retinal fundus image. It also helps to simplify the changes made after the rotation compared to the original one. The distribution of the colors in the space also helps to make learnability for the segmentation. Figure 15 depicts that the orientation of the color vector in the plot differs in every case of perpendicular rotation over three planes in the space.

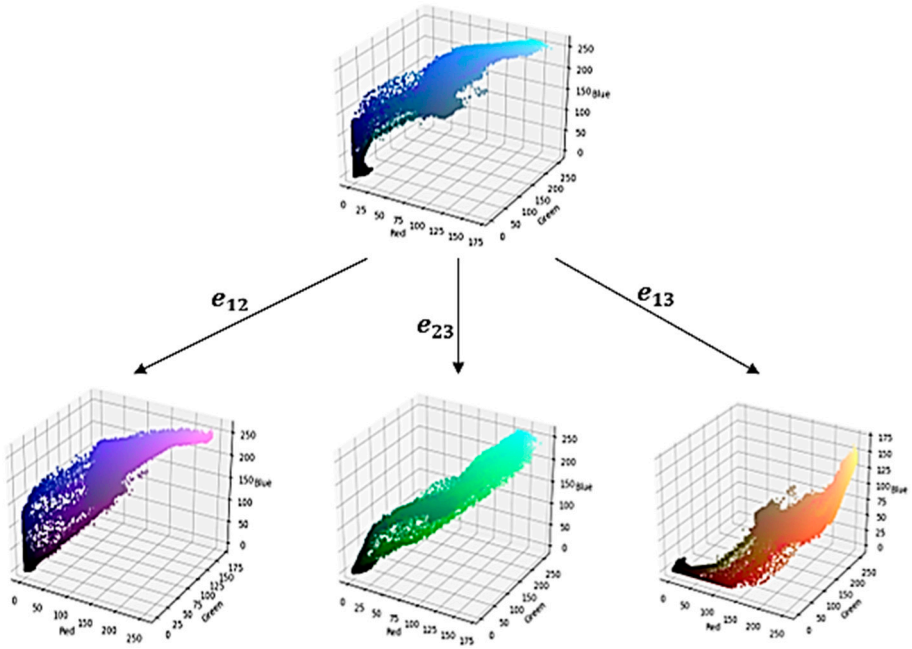

Figure 15. Plot-wise comparison for $\mathbf{90°}$ rotation.

A color histogram is a statistical representation of the distribution of colors within an image. It essentially counts the occurrence of each color value, displaying the results as a bar graph where the height of each bar corresponds to the frequency of that color. Unlike traditional bar graphs, the bars in a color histogram are adjacent, visually representing the color distribution's continuity. This visualization often reveals patterns resembling a normal distribution, indicating how colors are clustered and distributed throughout the image. This representation helps to realize the changeability of color features in the retinal fundus image. After rotation in $\mathbf{e_{12}}$ - plane, the red-green channel is swapped, forming a Magenta channel image. Green - Blue channel is swapped after rotation in $\mathbf{e_{23}}$ plane. It is represented as a yellow-green channel of the image. $\mathbf{e_{13}}$ - plane helps to represent the Cyan channeled image after the rotation and swapping of Red - Blue. Figure 16 below concludes the three scenarios discussed below.

© 2026 by the author(s). Distributed under a Creative Commons CC BY license.

Preprints.org (www.preprints.org) | NOT PEER-REVIEWED | Posted: 11 May 2026 doi:10.20944/preprints202605.0666.v1

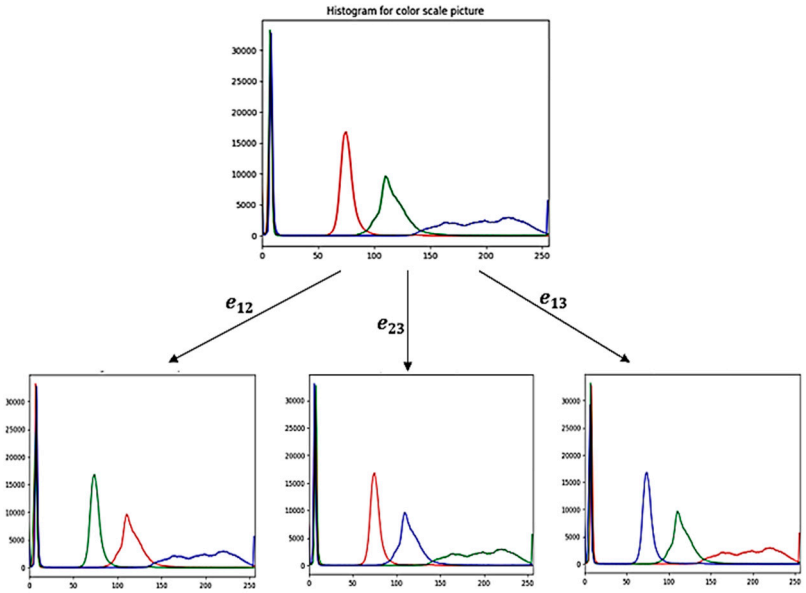

Figure 16. Histogram-wise comparison for $\mathbf{90°}$ rotation.

E. Observations on Image Representation

Extensive mathematical and experimental analysis has been conducted to investigate the impact of different rotation angles and axes on Clifford's color space representation of retinal fundus images. The results indicate that specific rotation angles can enhance image quality by optimizing color distribution. However, the optimal angle may vary depending on the specific image characteristics. Further research is needed to establish a robust methodology for determining the optimal rotation parameters for different image types and clinical applications.

1. After $\frac{\pi}{2}$ rotation, the retinal fundus image is transformed into a Cyan - Magenta - Yellow color model from the human preceptor's view.
2. The histogram bins are swapped after $\frac{\pi}{2}$ rotation on each plane. The Red - Green & Blue axes are exchanged while considering the bivector pairs.
3. The rotation on trivector or pseudoscalar doesn't make any impact as the whole space is spanned into $\mathbf{3}\mathbb{D}$ space.
4. The rotation at $\frac{\pi}{3}$ and $\frac{\pi}{4}$ are impacting all the representations, and color multivectors are not uniformly distributed. It is observed that the brightness property of the image is affected by different color expressions.
5. The selection of an accurate rotating axis and rotating angle may properly impact the image enhancement technique for subsequent retinal analysis.

The experiment is done on a novel color representation model tailored explicitly for retinal fundus images. By leveraging CA and the concept of color vector rotation, the method aims to improve image quality through effective color enhancement. The proposed model builds upon the existing HSI color space by incorporating angular information from the CA framework. This allows for detailed color manipulation and optimization, addressing the limitations of traditional color enhancement techniques. By treating color as a $\mathbf{Grade} - \mathbf{k}$ vector in a hexagonal plane defined by RGB and CMY color models, the method offers a flexible approach to image enhancement. The $\boldsymbol{rot_\theta}, \boldsymbol{rot_P}$ do not generalize a color image. These two factors categorically influence different applied areas of images for the betterment of image preprocessing.

6. Image Enhancement Using Clifford Color Rotor Mechanism

Color retinal images are the most frequent imaging data for screening and diagnosing eye illnesses, and they are often taken with fundus cameras. Exposure discomfort, machine parameter

© 2026 by the author(s). Distributed under a Creative Commons CC BY license.

Preprints.org (www.preprints.org) | NOT PEER-REVIEWED | Posted: 11 May 2026 doi:10.20944/preprints202605.0666.v1

setting problems, poor operations, and diverse medical staff experiences contribute to image acquisition. The present retinal image database contains several low-quality retinal images. Retinal image enhancement can improve the quality of retinal images, but it is necessary to process images representing color models and accurate mathematical idioms. The enhancement methodology is deployed to increase the quality of retinal images in ophthalmology clinics for consequent image processing steps and exact clinical diagnosis.

The proposed Clifford color rotor technique for retinal fundus image enhancement comprises six steps, excluding the inputted and finally enhanced image step, as depicted in Figure 17. The initial step of representation is discussed in the earlier section, which provides the foundation for this approach.

The input image is initially transformed into a Clifford color space, a mathematical representation that captures color and spatial information more comprehensively than traditional RGB color models. A suitable rotation angle $\boldsymbol{rot_\theta}$ is determined for subsequent image manipulation. This angle is crucial for optimizing the enhancement process. The image undergoes a bivector axis rotation by the determined angle, $\boldsymbol{rot_\theta}$. Several bivectors exist in Clifford's space. The most suitable plane for rotation $\boldsymbol{rot_P}$ is desired to be identified both mathematically and experimentally. This transformation aims to redistribute color information within the image. The rotated image is decomposed into its luminance and chrominance components. Luminance represents the overall brightness, while chrominance carries color information. The green channel of the luminance component is extracted and enhanced to improve contrast and detail [41]. The enhanced green channel is merged with the chrominance components, and the resulting image is reverse-rotated using the original angle $(\boldsymbol{\theta})$ to restore the original spatial orientation.

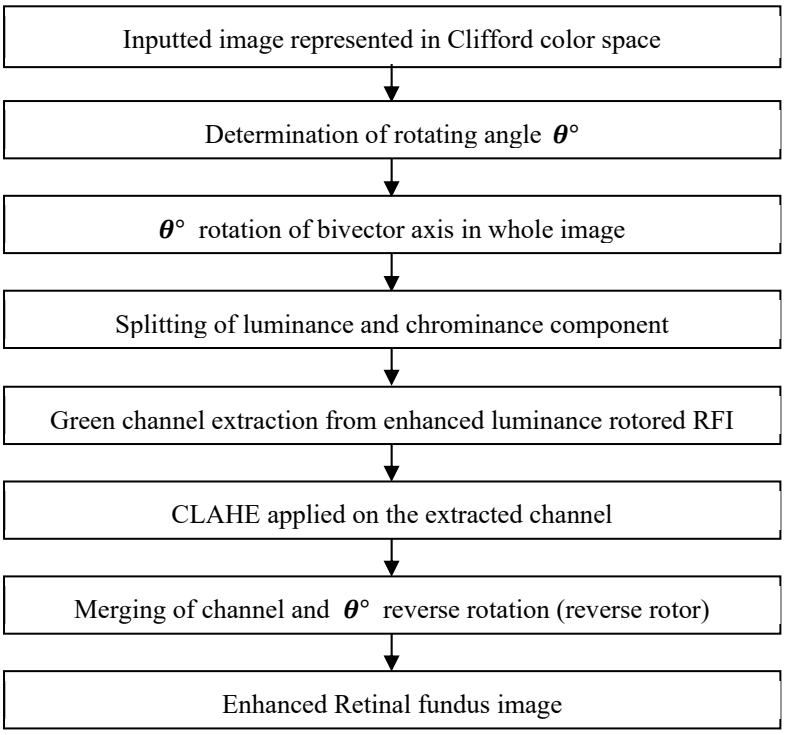

Figure 17. Retinal fundus image enhancement steps.

The optimal rotation plane and angle for enhancing retinal fundus images are determined through theoretical analysis and experimental evaluation. Discrete Entropy (DE), a measure of image information content, is employed to assess the effectiveness of different rotation parameters in restoring image details. By systematically varying the rotation plane and angle, the method seeks to identify the transformation that maximizes information preservation while enhancing visual clarity.

A. Impact of Angle of Rotation and Rotational Axis

© 2026 by the author(s). Distributed under a Creative Commons CC BY license.

Preprints.org (www.preprints.org) | NOT PEER-REVIEWED | Posted: 11 May 2026 doi:10.20944/preprints202605.0666.v1

The observations discussed in the earlier section about various degrees of rotation for multiple planes ensure the multivector representation of the retinal fundus image. It is perceived that the rotor function is responsible for the new color demonstration of the fundus and affects the image's intensity. An image's intensity change always refers to the alteration of illumination. The rotating angle plays a key role in increasing or decreasing intensity depending on the purpose or requirement. The following Figure 18 depicts the change of intensity for two different angles, $\frac{2\pi}{3}$ and $\frac{\pi}{4}$ in the same bivector axis.

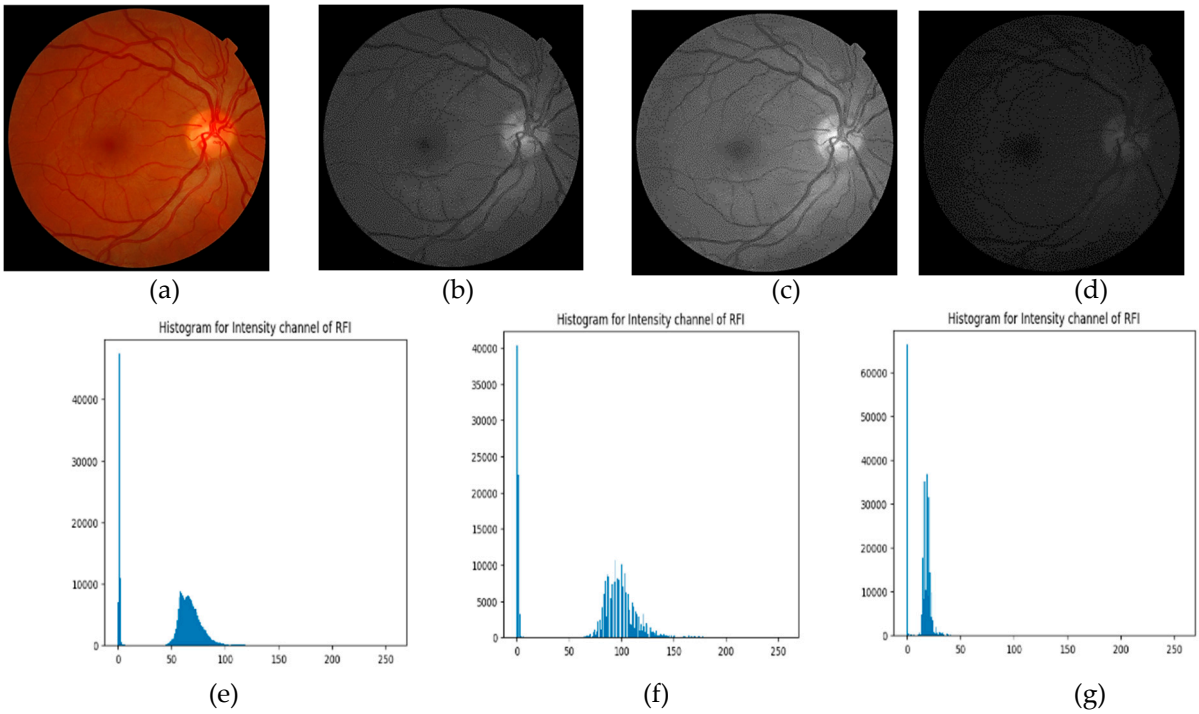

Figure 18. (a) Original RFI (b) Intensity image of original (c) $\frac{2\pi}{3}$ rotored intensity (d) $\frac{\pi}{4}$ rotored intensity (e) Histogram of the original image (f) $\frac{2\pi}{3}$ rotored intensity histogram (g) $\frac{\pi}{4}$ rotored intensity histogram.

B. Rotational Plane Generation

Based on the RGB color model with rotor operations, the Clifford color space shares similarities with the HSI color model. Both models aim to represent colors human-intuitively, separating intensity from color information. However, Clifford's color space offers a more geometric interpretation, utilizing CA for advanced color manipulations. While both models can be effective in image processing, their choice depends on specific application requirements and computational considerations.

In the observations stated earlier, it is said that Clifford's color space with the rotor mechanism is similar in that brightness is affected while the color multivectors are being rotated. Hence, if angular rotation is similar to Hue in the HSI model, then the intensity axis may work as a rotational plane. This plane is the gray-level axis spanned from scalar to pseudoscalar in Clifford color space shown in Figure 6. Hue represents the color itself, measured in degrees from $\mathbf{0}$ to $\mathbf{2\pi}$ degrees is Red, $\frac{2\pi}{3}$ degrees is Green, and $\frac{4\pi}{3}$ degrees is Blue. Cyan, Magenta, and Yellow are separated at $\frac{2\pi}{3}$ degree among each other. HSI is a hexagonal color model where the primary colors are separated at $\frac{\pi}{3}$ degree to each other. The rotor operator helps to rotate each color multivector maximum $\mathbf{2\pi}$ degree on the gray level axis. The primary colors, Red, Green, and Blue, are separated at $\frac{2\pi}{3}$ degree. It is expected a rotation about $\frac{2\pi}{3}$ degree from Red at $\mathbf{0°}$ degree in the anticlockwise direction will generate a Green component. Similarly, Blue can be formed for another $\frac{2\pi}{3}$ degree of rotation. Clifford's contribution is the bivector plane spanned between these color axes. The rotation of the

© 2026 by the author(s). Distributed under a Creative Commons CC BY license.

Preprints.org (www.preprints.org) | NOT PEER-REVIEWED | Posted: 11 May 2026 doi:10.20944/preprints202605.0666.v1

various **Grade – k** color vectors with respect to this bivector plane for the above-said angle defines the new color and changes in illumination.

Figure 19 shows two Grade – 1 vectors p and q forming a bivector $p \wedge q$ spanned between the color axes, e_r, e_g & e_b. The angle of rotation is $\frac{2\pi}{3}$ degree, which means that the vector $a = e_r + e_g$ will be rotated to $a' = e_r + e_b$, as shown in the figure below.

Hence, the rotor function $\mathcal{R}$ is rewritten as,

$$\mathcal{R} = \cos\frac{\theta}{2} + \mathbf{I}\sin\frac{\theta}{2} \tag{26}$$

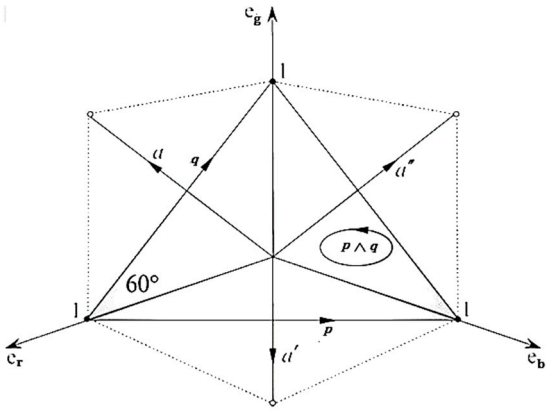

Figure 19. Rotor operation of a vector for $\frac{2\pi}{3}$ degree rotation.

Similarly, the reverse of a rotor is $\mathcal{R}^{-1}$,

$$\mathcal{R}^{-1} = \cos\frac{\theta}{2} - \mathbf{I}\sin\frac{\theta}{2} \tag{27}$$

Using Eq. (25), it is obtained,

$$\mathbf{X}_{rot} \mapsto (\cos\frac{\theta}{2} + \mathbf{I}\sin\frac{\theta}{2})(\mathbf{e}_r + \mathbf{e}_g)(\cos\frac{\theta}{2} - \mathbf{I}\sin\frac{\theta}{2}) \tag{28}$$

According to Figure 19, $a' = \mathbf{X}_{rot}$, and $\mathbf{I}$ has the role of unit bivector plane μ .
Hence,

$$a' = (\cos\frac{\pi}{3} + \mu\sin\frac{\pi}{3})(\mathbf{e}_r + \mathbf{e}_g)(\cos\frac{\pi}{3} - \mu\sin\frac{\pi}{3}) \tag{29}$$

$$= (\frac{1}{2} + \mu\frac{\sqrt{3}}{2})(\mathbf{e}_r + \mathbf{e}_g)(\frac{1}{2} + \mu\frac{\sqrt{3}}{2})$$

$$a' = \frac{1}{4}(1 + \mu\sqrt{3})(\mathbf{e}_r + \mathbf{e}_g)(1 - \mu\sqrt{3}) \tag{30}$$

Following Figure 19, it is specified that $p = \mathbf{e}_r - \mathbf{e}_b$ and $q = \mathbf{e}_r - \mathbf{e}_g$. Therefore, evaluating the outer product, the bivector $p \wedge q$ spanned between the color axes $\mathbf{e}_r, \mathbf{e}_g$ & $\mathbf{e}_b$ is,

$$p \wedge q = \mathbf{e}_{rg} + \mathbf{e}_{gb} + \mathbf{e}_{br} \tag{31}$$

A unit bivector μ as the rotating axis, which requires to rotate along $\frac{2\pi}{3}$ degree from a to a' is determined as,

$$\mu = \frac{\mathbf{e}_{rg} + \mathbf{e}_{gb} + \mathbf{e}_{br}}{\sqrt{3}} \tag{32}$$

© 2026 by the author(s). Distributed under a Creative Commons CC BY license.

Preprints.org (www.preprints.org) | NOT PEER-REVIEWED | Posted: 11 May 2026 doi:10.20944/preprints202605.0666.v1

Mathematically, it is obtained that for every $\frac{2\pi}{3}$ degree rotation, the rotational axis is $\boldsymbol{\mu}$ shown in Eq. (32). The Red, Green, and Blue colors are separated at the above-mentioned polar distance according to Clifford color space plotting on the HSI color model.

Following Figure 18, the observation that increasing the rotation angle in the Clifford color space leads to brighter retinal fundus images is consistent with the relationship between the rotation and the intensity component. By rotating the color vectors within the grayscale bivector axis, the technique effectively shifts the color distribution towards brighter regions of the color space, resulting in an overall increase in image illumination. This highlights the impact of color space transformations on image brightness and contrast. The general form of the multivector for gray value described in Eq. (20) is rewritten as a bivector axis component.

$$\mathcal{G} = \alpha \mathbf{e}_{\mathbf{rg}} + \beta \mathbf{e}_{\mathbf{gb}} + \gamma \mathbf{e}_{\mathbf{br}} \tag{33}$$

For $\alpha = \beta = \gamma$, the pixel is achromatic and is represented as a gray bivector axis. The Clifford color space is rotating on a bivector axis, representing a gray component. It resembles the HSI color model where the achromatic axis rotates 2π, its vector component, to generate luminance and chrominance properties. Hence, with the change in angle of rotation with the rotation axis $\mathbf{e}_{\mathbf{rg}} + \mathbf{e}_{\mathbf{gb}} + \mathbf{e}_{\mathbf{br}}$, which is a gray-level bivector that determines luminance and chrominance properties in the Clifford color space.

C. Determination of Angle of Rotation

The experiment seeks to evaluate the impact of different rotation angles and axes on the information content of retinal fundus images. By systematically varying these parameters, this study aims to identify the optimal combination for achieving the desired level of image enhancement. The focus on the grayscale bivector axis suggests that this particular axis is believed to be crucial for effectively manipulating color and brightness within the Clifford color space.

Entropy is a valuable metric for assessing image quality. It quantifies the amount of information or uncertainty present within an image. A higher entropy value generally indicates a more complex and detailed image, as more bits are required to represent its content accurately.

In image processing, discrete entropy is used to evaluate the information content of digital images. The complexity-details and quality can be assessed by measuring the entropy of an image. A higher entropy value suggests a more diverse and informative image, while a lower entropy value may indicate a simpler or noisier image.

The entropy is defined as,

$$\boldsymbol{E(I)} = -\sum_{k=1}^{L} \boldsymbol{p(k)} \log_2(\boldsymbol{p(k)}) \tag{34}$$

where $\boldsymbol{I}$ is the original image, $\boldsymbol{p(k)}$ is the probability of occurrence of the value $\boldsymbol{k}$ in the image $\boldsymbol{I}$, and $\boldsymbol{L} = \boldsymbol{2^q}$ indicates the number of different gray levels.

The information of the retinal fundus image after rotation with seven different angles in eight different subspaces is measured by entropy and depicted in Figure 20.

© 2026 by the author(s). Distributed under a Creative Commons CC BY license.

Preprints.org (www.preprints.org) | NOT PEER-REVIEWED | Posted: 11 May 2026 doi:10.20944/preprints202605.0666.v1

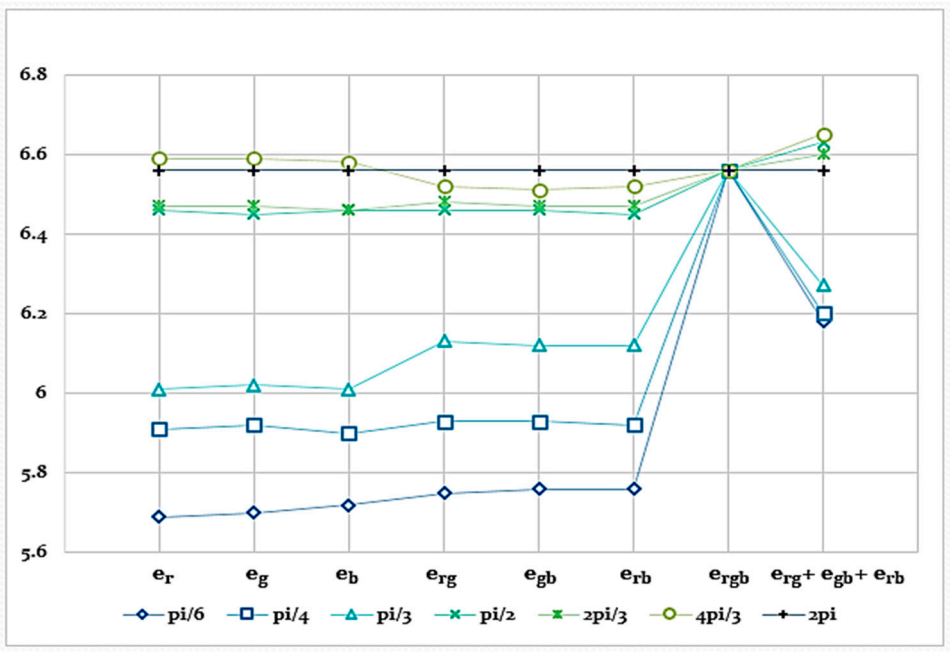

Figure 20. Image information performance on various rotating angles and subspaces.

The graph likely illustrates the entropy values of retinal fundus images after applying rotation operations at different angles with respect to other axes. The X-axis represents the different rotation angles used. The Y - axis displays the entropy values calculated for each image after rotation. All types of $\mathbf{Grade-k}$ vectors except $\mathbf{Grade-0}$ scalar components are considered here. Higher entropy values indicate greater information content and potentially better image quality, which is shown for the bivector axis $\frac{\mathbf{e_{12}+e_{23}+e_{31}}}{\sqrt{3}}$ with $\frac{4\pi}{3}$ degree rotation in Figure 20 above. The peaks in the graph are highlighting $\frac{4\pi}{3}$ degree rotation angles that enhance image detail or reduce noise. It is also experimented with pseudoscalar vectors $(\mathbf{e_{rgb}})$ the image shows no change of information despite various degrees of rotation, including $\frac{4\pi}{3}$.

The comparison graph of discrete entropy suggests the angle of rotation is $\frac{4\pi}{3}$ degree. While analyzing the value of the angle, it establishes that RGB colors are separated at $\frac{2\pi}{3}$ polar distance. The angle of rotation is considered $\frac{4\pi}{3}$ as the maximum span from Red to Blue according to Clifford color space based on the HSI color model. These basic colors are distributed at a distance of angle. $\frac{2\pi}{3}$, which is half of the determined angle, best fitted according to the rotor function for double reflection. Finally, the rotational axis is the bivector axis for optimal retinal fundus image enhancement. $\frac{\mathbf{e_{12}+e_{23}+e_{31}}}{\sqrt{3}}$ of Clifford color space and rotating angle is $\frac{4\pi}{3}$ degree.

D. Rotation Along the Bivector Axis

The rotation axis in Eq. (32) helps to express the rotation vector as,

$$\mathbf{R} = \boldsymbol{\cos\theta} + \frac{1}{\sqrt{3}}\boldsymbol{\mu}\boldsymbol{\sin\theta} = \boldsymbol{\cos\theta} + \frac{\mathbf{e_{12}+e_{23}+e_{31}}}{\sqrt{3}}\boldsymbol{\sin\theta} \tag{35}$$

The reverse of the rotation vector is,

$$\tilde{\mathbf{R}} = \boldsymbol{\cos\theta} - \frac{1}{\sqrt{3}}\boldsymbol{\mu}\boldsymbol{\sin\theta} = \boldsymbol{\cos\theta} - \frac{\mathbf{e_{12}+e_{23}+e_{31}}}{\sqrt{3}}\boldsymbol{\sin\theta} \tag{36}$$

The rotation of a color element $\mathbf{X}$ is expressed in Eq. (12) is rewritten, where $\mathbf{X} = \mathbf{re_1} + \mathbf{ge_2} + \mathbf{be_3}$. The rotation obtained,

© 2026 by the author(s). Distributed under a Creative Commons CC BY license.

Preprints.org (www.preprints.org) | NOT PEER-REVIEWED | Posted: 11 May 2026 doi:10.20944/preprints202605.0666.v1

$$\mathbf{R}\mathbf{X}\tilde{\mathbf{R}} = (\cos\boldsymbol{\theta} + \frac{\mathbf{e_{12}}+\mathbf{e_{23}}+\mathbf{e_{31}}}{\sqrt{3}}\sin\boldsymbol{\theta})\mathbf{X}(\cos\boldsymbol{\theta} - \frac{\mathbf{e_{12}}+\mathbf{e_{23}}+\mathbf{e_{31}}}{\sqrt{3}}\sin\boldsymbol{\theta}) \quad (37)$$

The above equation Eq. (37) is derived into three segments expressed below,

$$\mathbf{R}\mathbf{X}\tilde{\mathbf{R}} = \cos 2\boldsymbol{\theta}(\mathbf{r}\mathbf{e_1} + \mathbf{g}\mathbf{e_2} + \mathbf{b}\mathbf{e_3}) + \frac{2}{3}\sin^2\boldsymbol{\theta}\frac{\mathbf{e_{12}}+\mathbf{e_{23}}+\mathbf{e_{31}}}{\sqrt{3}}(\mathbf{r}+\mathbf{g}+\mathbf{b}) + \frac{1}{\sqrt{3}}\sin 2\boldsymbol{\theta}[(\mathbf{b}-\mathbf{g})\mathbf{e_{23}} + (\mathbf{r}-\mathbf{b})\mathbf{e_{31}} + (\mathbf{g}-\mathbf{r})\mathbf{e_{12}}] \quad (38)$$

The first term $\cos 2\boldsymbol{\theta}(\mathbf{r}\mathbf{e_1} + \mathbf{g}\mathbf{e_2} + \mathbf{b}\mathbf{e_3})$ is the Clifford color space component, second-term $\frac{2}{3}\sin^2\boldsymbol{\theta}\frac{\mathbf{e_{12}}+\mathbf{e_{23}}+\mathbf{e_{31}}}{\sqrt{3}}(\mathbf{r}+\mathbf{g}+\mathbf{b})$ is the intensity component, and the final term $\frac{1}{\sqrt{3}}\sin 2\boldsymbol{\theta}[(\mathbf{b}-\mathbf{g})\mathbf{e_{23}} + (\mathbf{r}-\mathbf{b})\mathbf{e_{31}} + (\mathbf{g}-\mathbf{r})\mathbf{e_{12}}]$ is the vector's color difference or chromaticity (hue and saturation). Eq. (38) demonstrates the general form of rotation using a gray-level bivector as the rotation axis. It also suggests that the rotation angle $\boldsymbol{\theta}$ is a crucial parameter in the proposed retinal image enhancement method. The choice of rotation angle significantly impacts the resulting image quality and the degree of color and brightness adjustments. It is possible to optimize image enhancement for specific tasks and desired outcomes by carefully selecting the appropriate rotation angle. Figure21 illustrates the change in color after the rotation operation.

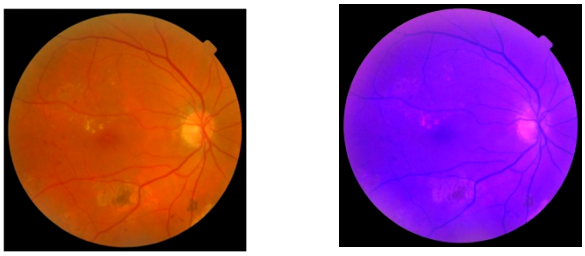

(a) (b)

Figure 21. (a) Inputted image in Clifford color space (b) Rotored image.

E. Splitting of Luminance and Chrominance Component

In the mathematical observation, for the angle of rotation $\boldsymbol{\theta} = \frac{\pi}{4}$, the first component $\cos 2\boldsymbol{\theta}(\mathbf{r}\mathbf{e_1} + \mathbf{g}\mathbf{e_2} + \mathbf{b}\mathbf{e_3})$ of color is diminished to zero and Clifford color space is mapped directly to HSI color space.

$$\mathbf{R}\mathbf{X}\tilde{\mathbf{R}} = \frac{1}{3}\boldsymbol{\mu}(\mathbf{r}+\mathbf{g}+\mathbf{b}) + \frac{1}{\sqrt{3}}[(\mathbf{b}-\mathbf{g})\mathbf{e_{23}} + (\mathbf{r}-\mathbf{b})\mathbf{e_{31}} + (\mathbf{g}-\mathbf{r})\mathbf{e_{12}}] \quad (39)$$

The above equation Eq. (39) is reduced into two parts, where $\frac{1}{3}\boldsymbol{\mu}(\mathbf{r}+\mathbf{g}+\mathbf{b})$ is luminance and $\frac{1}{\sqrt{3}}[(\mathbf{b}-\mathbf{g})\mathbf{e_{23}} + (\mathbf{r}-\mathbf{b})\mathbf{e_{31}} + (\mathbf{g}-\mathbf{r})\mathbf{e_{12}}]$ suggests the chrominance property of the color after rotation. Hence, it is established that any change of chromaticity is the shift of hue for an angle greater than $\frac{\pi}{4}$. The angle of rotation $\boldsymbol{\theta}° = \frac{4\pi}{3}$ is considered and applied on each color pixel of the retinal fundus image. The blue representation of the retinal fundus image is depicted in Figure 21(b), suggesting the rotation's correctness. The blue component is separated at a distance of $\frac{4\pi}{3}$ degree in the HSI model. The luminance component of the retinal fundus images increased after rotation along the bivector axis. It suggests that this transformation effectively enhanced the overall brightness or intensity of the images. This could be beneficial for improving the visibility of delicate details or features within the retinal structures. Figure 22 demonstrates the changes made in the luminance and chrominance components of the rotored image.

© 2026 by the author(s). Distributed under a Creative Commons CC BY license.

Preprints.org (www.preprints.org) | NOT PEER-REVIEWED | Posted: 11 May 2026 doi:10.20944/preprints202605.0666.v1

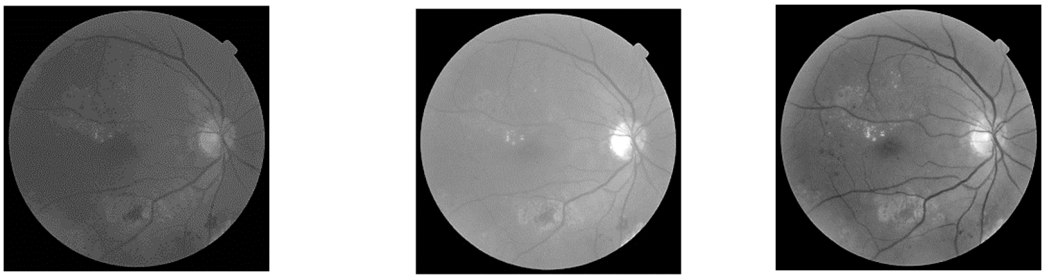

(a) (b) (c)

Figure 22. (a) Original intensity (b) Luminance component (c) Chrominance component.

F. Luminance Correction

The enhanced luminance component illuminated the whole image after rotation, and Contras Limited Adaptive Histogram Equalization (CLAHE) was applied to the green channel component to illuminate the whole image uniformly. It is a powerful image enhancement technique that can significantly improve the visibility of details in retinal fundus images. The green channel is often preferred for image enhancement due to its higher information content and reduced noise than the red and blue channels [1]. The green channel is merged with red and blue components. Figure 23 (a) depicts the uniformly illuminated rotored retinal fundus image.

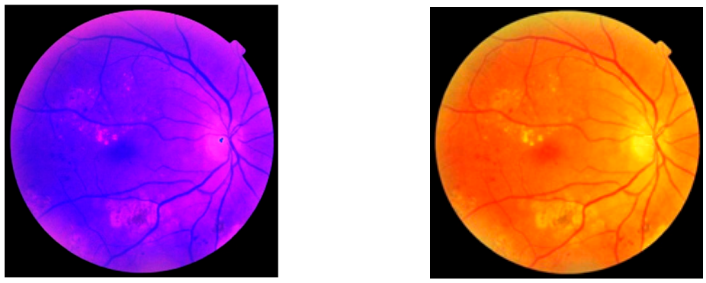

(a) (b)

Figure 23. (a) Enhanced rotored retinal fundus image (b) Enhanced retinal fundus image.

In the final step, the rotored image is reversed back to its original colored description with enhancement. The reverse rotation is expressed as the equation given below.

$$\tilde{\mathbf{R}}\mathbf{X}\mathbf{R} = (\cos\boldsymbol{\theta} - \frac{\mathbf{1}}{\sqrt{\mathbf{3}}}\boldsymbol{\mu}\sin\boldsymbol{\theta})\mathbf{X}(\cos\boldsymbol{\theta} + \frac{\mathbf{1}}{\sqrt{\mathbf{3}}}\boldsymbol{\mu}\sin\boldsymbol{\theta}) \quad (40)$$

For, $\boldsymbol{\theta} = \frac{\boldsymbol{\pi}}{\mathbf{4}}$, the reverse rotor equation is reduced to two terms, as regular rotation operation is shown in Eq. (41).

$$\frac{\mathbf{1}}{\mathbf{3}}\boldsymbol{\mu}(\mathbf{r}+\mathbf{g}+\mathbf{b}) - \frac{\mathbf{1}}{\sqrt{\mathbf{3}}}[(\mathbf{b}-\mathbf{g})\mathbf{e_{23}} + (\mathbf{r}-\mathbf{b})\mathbf{e_{31}} + (\mathbf{g}-\mathbf{r})\mathbf{e_{12}}] \quad (41)$$

The nature of luminance and chrominance is preserved for $\boldsymbol{\theta}°$ $(= \frac{\mathbf{4\pi}}{\mathbf{3}})$ rotation and the bivector axis in the actual retinal fundus image result. Figure 23 (b) shows that the method proposed in this literature successfully enhances retinal fundus images by combining Clifford color space transformations and enhancement.

7. Experimental Results

© 2026 by the author(s). Distributed under a Creative Commons CC BY license.

Preprints.org (www.preprints.org) | NOT PEER-REVIEWED | Posted: 11 May 2026 doi:10.20944/preprints202605.0666.v1

The proposed enhancement technique is implemented on the DRIVE [42] and MESSIDOR [43] data sets. Table 1 specifies the datasets of retinal images employed for representation and enhancement.

Table 1. Specification for DRIVE and MESSIDOR datasets.

Dataset Name	Dataset Size	FOV	Image Size (pixels)	Images Format	Ground Truth
DRIVE (2004)	40 images (two sets)	45°	565 × 584 (both sets)	TIFF	Blood Vessels
MESSIDOR (2004)	1200 images (three sets)	45°	Set(1): 1440 × 960 Set(2): 2240 × 1488 Set(3): 2304 × 1536	TIFF	Retinopathy Grading and Macular Edema (Hard Exudates)

Figures 24 & 25 compare the original input image in Clifford color space, rotored image, enhanced rotored image, and final enhanced image, along with a comparison between the intensity of the input image and the rotored intensity image, respectively.

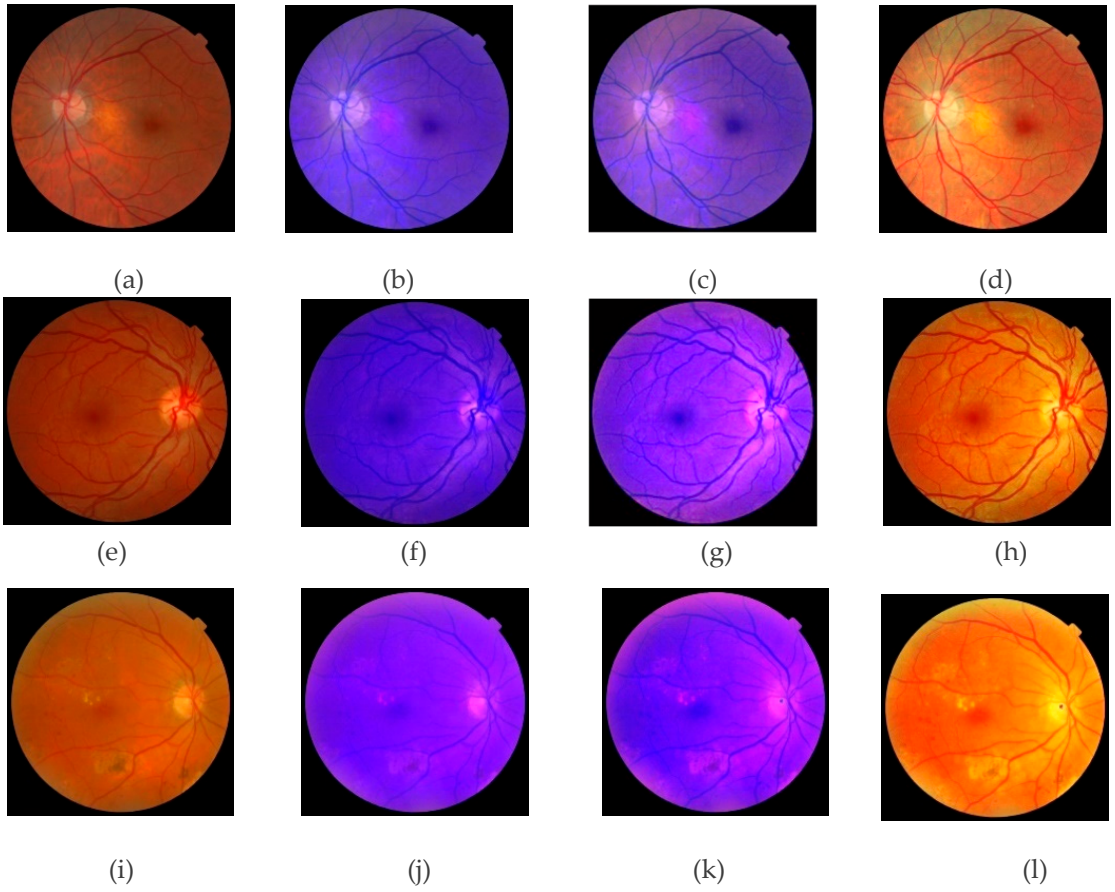

(a) (b) (c) (d)

(e) (f) (g) (h)

(i) (j) (k) (l)

© 2026 by the author(s). Distributed under a Creative Commons CC BY license.

Preprints.org (www.preprints.org) | NOT PEER-REVIEWED | Posted: 11 May 2026 doi:10.20944/preprints202605.0666.v1

Figure 24. (a), (e), (i) Input image in Clifford color space (b), (f), (j) Rotored image (c), (g), (k) Enhanced rotored image (d), (h), (l) Final enhanced image.

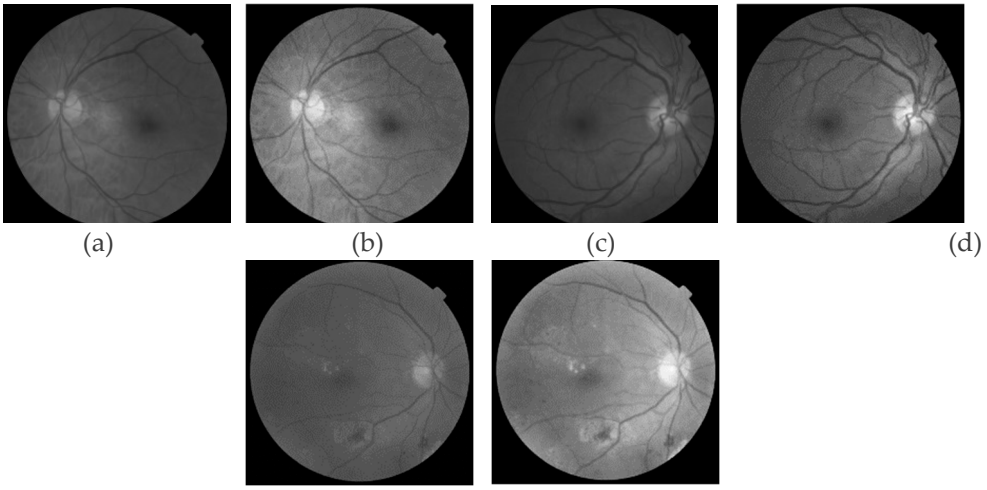

Figure 25. (a), (c), (e) Input image intensity (b), (d), (f) Rotored image intensity.

8. Performance Evaluation

The program code for the proposed method was developed in Python 3 Google's compute engine backend, which has 16 GB RAM and 500 GB disk with Intel(R) Xeon(R) CPU at 2.20GHz (two virtual CPUs). Table 2 tabulates the performance comparison of retinal image enhancement techniques in the DRIVE and MESSIDOR datasets. The performance of the existing techniques with the proposed methodology is evaluated on the datasets mentioned above in terms of the following metrics - Peak-to-signal noise ratio (PSNR) and Discrete Entropy (DE). The similarity of the original input image and enhanced images' similarity is evaluated using the Structural Similarity Index measure (SSIM). Peak Signal-to-Noise Ratio (PSNR) measures image quality based on pixel-wise differences between the original and enhanced images. Higher PSNR values indicate better image quality with less noise. Discrete entropy (DE) is discussed earlier in this paper when determining the rotating angle and axis. It is also used as a metric for quantifying information content or randomness in an enhanced retinal fundus image. Higher DE values suggest a more complex and detailed image. The SSIM is a perceptual metric that considers factors like luminance, contrast, and structure.

The considered metrics are calculated using Eqs. (42) – (44) for Clifford color space-based image representation and enhancement. PSNR is a logarithmic transformation of the reciprocal of the Mean Square Error (MSE) metric. A lower MSE (indicating a more minor difference between the images) leads to a higher PSNR, suggesting better image quality. MSE is a commonly used metric to quantify the difference between two images. It calculates the average squared difference between corresponding pixels in the original and resulting images.

$$\mathbf{MSE} = \frac{\mathbf{1}}{\mathbf{mn}} \sum_{\mathbf{i=0}}^{\mathbf{m-1}} \sum_{\mathbf{j=0}}^{\mathbf{n-1}} [\mathbf{Y(i,j)} - \mathbf{X(i,j)}]^{\mathbf{2}} \tag{42}$$

where $\mathbf{X}$ and $\mathbf{Y}$ represent enhanced and input images, respectively; $\mathbf{m}$ and $\mathbf{n}$ represent the number of rows and columns in the images.

PSNR is considered in this literature as it provides a more intuitive and interpretable measure of image quality than MSE and is expressed in decibels (dB).

$$\mathbf{PSNR} = \mathbf{10}\,\mathbf{log_{10}}\left(\frac{\mathbf{R^2}}{\mathbf{MSE}}\right) \tag{43}$$

where $\mathbf{R}$ represents the maximum fluctuation present in the inputted retinal fundus image.

© 2026 by the author(s). Distributed under a Creative Commons CC BY license.

Preprints.org (www.preprints.org) | NOT PEER-REVIEWED | Posted: 11 May 2026 doi:10.20944/preprints202605.0666.v1

$$\mathbf{SSIM}(\mathbf{x},\mathbf{y}) = \mathbf{l}(\mathbf{x},\mathbf{y}) * \mathbf{c}(\mathbf{x},\mathbf{y}) * \mathbf{s}(\mathbf{x},\mathbf{y}) \quad (44)$$

where $\mathbf{l}(\mathbf{x},\mathbf{y})$, $\mathbf{c}(\mathbf{x},\mathbf{y})$, $\mathbf{s}(\mathbf{x},\mathbf{y})$ represents luminance, contrast, and structure comparison between input $(\mathbf{x})$ and enhanced $(\mathbf{y})$ images.

Discrete Entropy (DE) is defined in Eq. (34) as $\boldsymbol{E}(\boldsymbol{I})$, where $\boldsymbol{I}$ is the inputted image.

The performance of the proposed enhancement technique is evaluated using performance measures such as PSNR, DE, and SSIM. The proposed methodology achieved 29.83 dB and 7.13 while measuring the PSNR and DE metrics. The proposed image enhancement technique demonstrates superior performance compared to existing methods in terms of PSNR and DE, indicating improved image quality and information preservation.

However, it falls slightly behind in SSIM, suggesting potential limitations in preserving structural similarity compared to the existing quantile-based techniques (for q =5) proposed by Gupta et al. [3]. Overall, the method is valuable for retinal image representation and enhancement.

Table 2. Comparison of enhancement performance with existing literature for MESSIDOR and DRIVE datasets.

Methods	PSNR	SSIM	DE
Zhou et al. [8]	23.11	0.58	5.67
Gupta et al. [3] (for q=3)	27.67	0.66	5.68
Gupta et al. [3] (for q=5)	28.40	**0.69**	5.66
Priyadarshini et al. [1]	27.79	0.63	7.07
Proposed method	**29.83**	0.68	**7.13**

The following chart depicted in Figure 26 exhibits the performance of this research with recent literature only for the DRIVE dataset. The results show that the proposed enhancement technique outperforms the three considered methods by achieving higher PSNR & DE values.

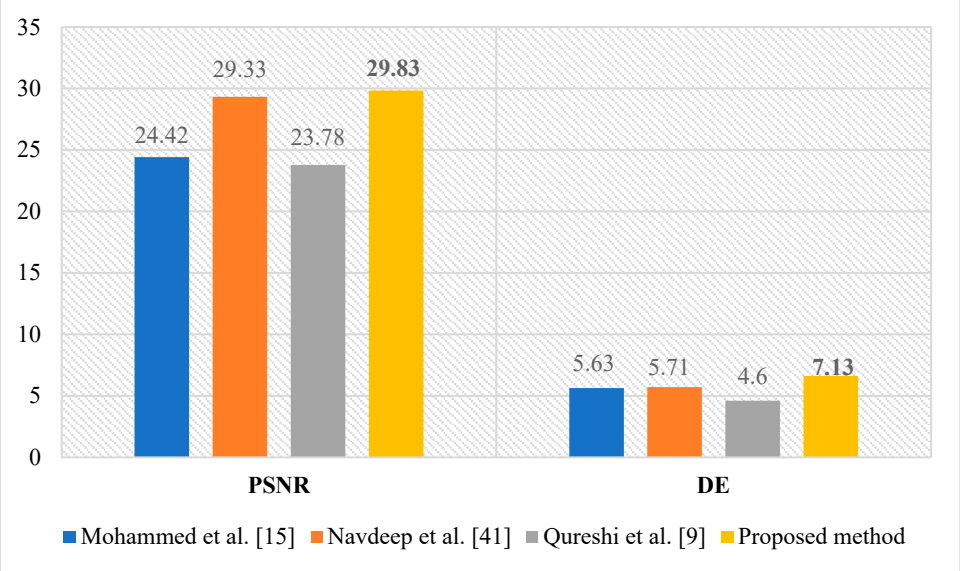

Figure 26. PSNR and Entropy measure comparison of DRIVE dataset.

9. Conclusion

© 2026 by the author(s). Distributed under a Creative Commons CC BY license.

Preprints.org (www.preprints.org) | NOT PEER-REVIEWED | Posted: 11 May 2026 doi:10.20944/preprints202605.0666.v1

Retinal image enhancement is an essential step under the preprocessing stage to view the retinal anomalies better and identify the type of disease a patient suffers. This research work is divided into two parts - image representation and enhancement. The representation of the fundus image is made in a Clifford color space. It is a unique $\mathbb{3D}$ color space based on the RGB color model. This color space stores each color in the form of an individual multivector. The multivectors are the geometric entities of CA. They hold the color information and also preserve the luminance feature. The rotation operation is applied to these color multivectors to correct the illumination of the fundus images. The deviations occurred in the image's brightness and color data. The rotating angle and the rotational axis are decisive parameters for the accurate enhanced image. The gray level axis is considered the rotational plane where all the multivectors are being rotated at a certain angle for the color and brightness correction in the images. The choice of the rotational angle plays a significant role where the brightness or contrast properties may face impact like over-illuminated or under-illuminated. The angle $\frac{4\pi}{3}$ and grayscale bivector as the rotational axis is determined mathematically and experimentally using discrete entropy (DE). The green channel is extracted from the rotored luminance component. The CLAHE technique is applied to enhance the selected channel. Finally, the channel is merged back to the other two color channels. The enhanced rotored fundus images are reversely rotated to the original color representation and uniformly illuminated.

The proposed image enhancement technique's effectiveness is evaluated using standard metrics: peak signal-to-noise ratio (PSNR), discrete entropy (DE), and structural similarity index measure (SSIM). These metrics are applied to the MESSIDOR and DRIVE datasets. The results demonstrate that the proposed approach significantly outperforms existing methods by achieving higher PSNR and DE values, indicating improved image quality and information preservation. The proposed method for enhancing images is particularly effective for retinal landmark and lesion detection, which involves analyzing fundus images in terms of physical and mechanical properties.

Availability of Data and Material: The datasets accessed and analyzed during the current study are available in the MESSIDOR [43] (https://doi.org/10.5566/ias.1155), and DRIVE [42] repository (https://drive.grand-challenge.org/).

Competing Interests: The authors declare that they have no competing interests. Any interest or relationship, financial or otherwise, that might be perceived as influencing the authors' objectivity is considered a potential source of conflict of interest.

Acknowledgments: The authors sincerely thank the Department of Computer Science and Engineering, University of Calcutta West Bengal, India and Sister Nivedita University, West Bengal, India for using the infrastructure facilities to develop the technique.

References

1. Priyadharsini, C. "Retinal image enhancement based on color dominance of image." Scientific Reports 13 (2023).
2. G. Nayomi, R. Ranamuka, N. Gayan, Meegama, Detection of hard exudates from diabetic retinopathy images using fuzzy logic, 2013, IET Image Processing, Vol. 7, 2, pp. 121–130.
3. Gupta, Bhupendra, & Mayank Tiwari. "Color retinal image enhancement using luminosity and quantile-based contrast enhancement." Multidimensional Systems and Signal Processing 30, no. 4 (2019): 1829- 1837.
4. Somasis Roy, Anirban Mitra ,Sanjit Kumar Setua, "Color Image Representation Using Multivector", IEEE 2014 Fifth International Conference on Intelligent Systems, Modelling and Simulation (ISMS 2014) ,Date of Conference: 27-29 Jan. 2014,Date Added to IEEE Xplore: 01 October 2015, INSPEC Accession Number: 15507901,DOI: 10.1109/ISMS.2014.66,Publisher: IEEE
5. Yin X-X, Hadjiloucas S, Zhang Y (2017) Outlook for Clifford Algebra Based Feature and Deep Learning AI Architectures. Pattern Classification of Medical Images: Computer Aided Diagnosis. Springer, Cham, pp. 165–177

© 2026 by the author(s). Distributed under a Creative Commons CC BY license.

Preprints.org (www.preprints.org) | NOT PEER-REVIEWED | Posted: 11 May 2026 doi:10.20944/preprints202605.0666.v1

6. Roy, Somasis, Anirban Mitra, Sudipta Roy, and Sanjit Kumar Setua. "Blood vessel segmentation of retinal image using Clifford matched filter and Clifford convolution." Multimedia Tools and Applications 78 (2019): 34839-34865.
7. Mishra B, Wilson P, Al-Hashimi BM (2008) Advancement in color image processing using Geometric Algebra. Signal Processing Conference, 2008 16th European. IEEE
8. Zhou, M., Jin, K., Wang, S., Ye, J. & Qian, D. Color retinal image enhancement based on luminosity and contrast adjustment. IEEE Trans. Biomed. Eng. 65(3), 521– 527. https:// doi. org/ 10.1109/ TBME. 2017. 27006 27 (2018).
9. Qureshi, I., Ma, J. & Shaheed, K. A hybrid proposed fundus image enhancement framework for diabetic retinopathy. Algorithms 12(1), 14. https:// doi. org/ 10.3390/ a1201 0014 (2019).
10. Alwazzan, M. J., Ismael, M. A. & Ahmed, A. N. A hybrid algorithm to enhance colour retinal fundus images using a wiener filter and CLAHE. J. Digit. Imaging 34(3),750–759. https:// doi. org/ 10. 1007/ s10278- 021- 00447-0 (2021).
11. A. Sopharak, A.Uyyanonvara, Automatic Exudates Detection from Non-Dilated Diabetic Retinopathy Retinal Images using Fuzzy C-means Clustering, 2009, Sensors, pp. 2148-2161.
12. M. Iqbal, A. Aibinu, Detection of Vascular intersection in retinal fundus Image using Modified Cross point number and NN Technique, 2008, Int. Conf. Comp. Comm. Engg, pp. 241 - 246.
13. Kumar, R. & Kumar Bhandari, A. Luminosity and contrast enhancement of retinal vessel images using weighted average histogram. Biomed. Signal Process. Control 71, 103089. https:// doi. org/ 10. 1016/j. bspc. 2021. 103089 (2022).
14. Palanisamy, G., Ponnusamy, P. & Gopi, V.P. An improved luminosity and contrast enhancement framework for feature preservation in color fundus images. SIViP 13, 719–726(2019). https://doi.org/10.1007/s11760- 01 8-1401 -y
15. Jawad, E. M., Hazim, H. J. M. & Daway, G. Retinal image enhancement by using adapted histogram equalization based on segmentation and lab color space. Int. J. Intell. Eng. Syst. 15(3), 614–622. https:// doi. org/ 10. 22266/ ijies 2022. 0630. 52 (2022).
16. Dissopa, J., Kansomkeat, S. & Intajag, S. Enhance contrast and balance color of retinal image. Symmetry 13(11), 2089. https:// doi.org/ 10. 3390/ sym13 112089 (2021).
17. Dai, P., Sheng, H., Zhang, J., Li, L., Wu, J., & Fan, M. (2016). Retinal fundus image enhancement using the normalized convolution and noise removing. International journal of biomedical imaging, 2016.
18. A Anilet Bala et al 2021 J. Phys.: Conf. Ser. 1964 062034
19. Shamsudeen, Fousia M., and G. Raju. "An objective function based technique for devignetting fundus imagery using MST." Informatics in Medicine Unlocked 14 (2019):82-91.
20. Joshi, Shilpa, and P. T. Karule. "Review of preprocessing techniques for fundus image analysis." Advances in Modelling and Analysis B 60.3 (2018): 593-612.
21. Wang, Jianglan, Yong-Jie Li, and Kai-Fu Yang. "Retinal fundus image enhancement with image decomposition and visual adaptation." Computers in Biology and Medicine 128 (2021): 104116.
22. Bindhya, P., Chitra Jegan, and V. Raj. "A Review on Methods of Enhancement and Denoising in Retinal Fundus Images." INTERNATIONAL JOURNAL OF COMPUTER SCIENCES AND ENGINEERING 8 (2020): 1-9.
23. Yavuz, Z., & Köse, C." Blood vessel extraction in color retinal fundus images with enhancement filtering and unsupervised classification" Journal of healthcare engineering, Vol.8, Issue.3, 2017.
24. Mittal, Kanupriya, and V. Mary Anita Rajam. "Computerized retinal image analysis-a survey." Multimedia tools and Applications 79.31 (2020): 22389-22421.
25. Kandpal, A.; Jain, N. Retinal Image Enhancement Using Edge-based Texture Histogram Equalization. In Proceedings of the International Conference on Signal Processing and Integrated Networks, Noida, India, 27–28 February 2020.
26. Gaudio, A.; Smailagic, A.; Campilho, A. Enhancement of Retinal Fundus Images via Pixel Color Amplification. In Proceedings of the 17th International Conference, ICIAR 2020, Póvoa de Varzim, Portugal, 24–26 June 2020.

© 2026 by the author(s). Distributed under a Creative Commons CC BY license.

Preprints.org (www.preprints.org) | NOT PEER-REVIEWED | Posted: 11 May 2026 doi:10.20944/preprints202605.0666.v1

27. Latif J, Xiao C, Imran A, Tu S. "Medical imaging using machine learning and deep learning algorithms: a review," in 2019 2nd International Conference on Computing, Mathematics and Engineering Technologies (iCoMET). Sukkur, (2019). p. 1–5.
28. Ma Y, Liu J, Liu Y, Fu H, Hu Y, Cheng J, et al. Structure and illumination constrained GAN for medical image enhancement. IEEE Trans Med Imag. (2021) 40:3955–3967. doi: 10.1109/TMI.2021.3101937
29. Hemelings R, Elen B, Stalmans I, Van Keer K, De Boever P, Blaschko MB. Artery–vein segmentation in fundus images using a fully convolutional network. Comput Med Imag Graph. (2019) 76:101636. doi: 10.1016/j.compmedimag.2019.05.004
30. Farooq U, Sattar NY. "Improved automatic localization of optic disc in Retinal Fundus using image enhancement techniques and SVM," in 2015 IEEE International Conference on Control System, Computing and Engineering (ICCSCE) (2015). (Penang), p. 532–537.
31. Zhao H, Yang B, Cao L, Li H. Chapter 9. In: Data-Driven Enhancement of Blurry Retinal Images via Generative Adversarial Networks. Lecture Notes in Computer Science (2019). p. 75–83.
32. You Q, Wan C, Sun J, Shen J, Ye H, Yu Q. "Fundus Image Enhancement Method Based on CycleGAN," in 2019 41st Annual International Conference of the IEEE Engineering in Medicine and Biology Society (EMBC) (Berlin). (2019).
33. Almotiri, J., Sivaswamy, J., & Akram, M. U. (2016). A Vectorized Structure Tensor Approach for Retinal Vessel Segmentation. IEEE Transactions on Medical Imaging, 35(2), 672-683.
34. Zhang, J., Zhang, J., Zhang, L., & Peng, H. (2016). Retinal vessel enhancement based on directional filter bank and local binary patterns. IEEE Access, 4, 6130- 6140.
35. Miri, M. S., & Mahlooji Far, A. (2015). A novel multi-level vector ordering and adaptive thresholding algorithm for optic disc detection. Journal of Medical Signals & Sensors, 5(1), 23-33.
36. Lee, K. W., & Wu, X. (2015). Retinal vessel segmentation using L1 regularized deep sparse filtering. In 2015 IEEE 12th International Symposium on Biomedical Imaging (ISBI) (pp. 417-420). IEEE.
37. Rangrej, J., & Shah, N. (2017). Improved optic disc detection using novel hybrid approach. Procedia Computer Science, 105, 203-208.
38. L.Dorst and S.Mann. "Geometric algebra: A computational framework for geometrical applications (part I)". IEEE Computer Graphics and Applications, (Volume: 22, Issue:3), pp. 24-31,2002.
39. Franchini, Silvia, et al. "Clifford Algebra Based Edge Detector for Color Images." Complex, Intelligent and Software Intensive Systems (CISIS), 2012 Sixth International Conference on. IEEE, 2012.
40. S.J.Sangwine and T.A.EII, "Colour image filters based on hypercomplex convolution", Vision, Image and Signal Processing, IEE Proceedings - Volume:147 , Issue: 2, pp. 89 – 93, Apr 2000
41. Singh, N., Kaur, L. & Singh, K. Histogram equalization techniques for enhancement of low radiance retinal images for early detection of diabetic retinopathy. Eng. Sci. Technol. Int. J. 22(3), 736–745. https:// doi. org/ 10. 1016/j. jestch. 2019. 01. 014 (2019).
42. J. Staal, M. D. Abramoff, M. Niemeijer, M. A. Viergever and B. van Ginneken, "Ridge- based vessel segmentation in color images of the retina," in IEEE Transactions on Medical Imaging, vol. 23, no. 4, pp. 501-509, April 2004, doi: 10.1109/TMI.2004.825627
43. E. Decencière, X. Zhang, G. Cazuguel et al., "Feedback on a publicly distributed image database: the Messidor database," Image Analysis & Stereology, vol. 33, no. 3, pp. 231

Disclaimer/Publisher's Note: The statements, opinions and data contained in all publications are solely those of the individual author(s) and contributor(s) and not of MDPI and/or the editor(s). MDPI and/or the editor(s) disclaim responsibility for any injury to people or property resulting from any ideas, methods, instructions or products referred to in the content.

© 2026 by the author(s). Distributed under a Creative Commons CC BY license.